Measures of population immunity can predict the dominant clade of influenza A (H3N2) and reveal age-associated differences in susceptibility and specificity

Kangchon Kim[1*], Sigrid Gouma[2], Marcos C. Vieira[1], Madison E. Weirick[2], Scott E. Hensley[2], and Sarah Cobey[1]

1 Department of Ecology and Evolution, The University of Chicago, USA
2 Department of Microbiology, Perelman School of Medicine, The University of Pennsylvania, USA

* kangchonsara@gmail.com

Abstract

For antigenically variable pathogens such as influenza, strain fitness is partly determined by the relative availability of hosts susceptible to infection with that strain compared to others. Antibodies to the hemagglutinin (HA) and neuraminidase (NA) confer substantial protection against influenza infection. We asked if a cross-sectional antibody-derived estimate of population susceptibility to different clades of influenza A (H3N2) could predict the success of clades in the following season. We collected sera from 483 healthy individuals aged 1 to 90 years in the summer of 2017 and analyzed neutralizing responses to the HA and NA of representative strains. The clade to which neutralizing antibody titers were lowest, indicating greater population susceptibility, dominated the next season. Titers to different HA and NA clades varied dramatically between individuals but showed significant associations with age, suggesting dependence on correlated past exposures. Despite this correlation, inter-individual variability in antibody titers to H3N2 strains increased gradually with age. This study indicates how representative measures of population immunity might improve evolutionary forecasts and inform selective pressures on influenza.

Author summary

The rapid evolution of influenza requires semi-annual updates to the strains included in influenza vaccines. New vaccine strains are frequently chosen based on their ability to escape immunity to other strains, with the degree of escape estimated from experimental infections of ferrets. However, the cross-reactivity derived from ferret experiments does not always match measures in people, who often have a long history of influenza exposures. We conducted a large cross-sectional serological study involving 483 individuals between 1 and 90 years of age and tested their sera against the major surface protein of eight circulating influenza strains. Levels of neutralizing antibody successfully predicted the dominant strain in the next influenza season. Different age groups showed different patterns of binding, although there was substantial variability in responses within age groups and an increase in the diversity of neutralizing antibody profiles with age. Our study demonstrates the feasibility of using cross-sectional sera to estimate major selection pressure on influenza.

Introduction

The epidemiological and evolutionary dynamics of antigenically variable pathogens are intrinsically sensitive to immunity in the host population. This understanding has long shaped vaccination strategies against influenza. Twice each year, representative strains from circulating clades are evaluated for their ability to escape antibodies to current vaccine strains, under the expectation that these clades might come to dominate and could be poorly matched by the current vaccine. As surrogates for the human population, influenza-naive ferrets are infected or vaccinated with one of a set of reference influenza strains (e.g., current vaccine strains), and their post-exposure sera are tested against candidate strains for the next vaccine. The extent to which these sera cross-react or neutralize candidate strains is taken as a measure of their immune escape or antigenic distance [1, 2]. These experimental measures of immune escape, alongside other estimates of variant growth rates and sequence-based fitness models [3], are used to anticipate the dominant clade and need for vaccine updates. In the past few years, escape from human sera has been considered too (e.g., [4]).

An open question is whether more direct and representative estimates of population immunity could lead to better vaccine choices while potentially shedding light on the mechanisms of coevolution between the viral population and host immunity. In the past decade, large differences have occasionally appeared in the antigenic distances inferred from ferret compared to human sera [5, 6]. It's possible that these differences arise at the species level, although the antibody responses of ferrets and humans after their first influenza exposures appear roughly similar [7]. A more likely explanation comes from the observation of original antigenic sin, whereby individuals exposed to the same strain of influenza can mount antibody responses with different cross-reactivity profiles shaped by their distinct histories of exposure [5, 8–11]. These past infections and vaccinations lead to biases in which viral sites or epitopes antibodies recognize. Consequently, a mutation in one epitope might be antigenically important for some people (or ferrets) but not others. Since most influenza infections occur in people with preexisting immunity to influenza, and antibodies to influenza surface proteins contribute substantially to protection (and transmission) [5, 12–16], accurate measures of population immunity may be useful in viral forecasting and vaccine strain selection.

Using the 2017-2018 influenza season in North America as a case study, we characterized a cross-sectional, age-representative estimate of antibody-mediated immunity in an urban population and asked whether it could predict which of several circulating clades of H3N2 would dominate regionally in the next influenza season. Forecasting for vaccine strain selection often focuses on antigenic changes to the hemagglutinin (HA) surface protein, which vaccines attempt to match. We measured neutralizing antibody titers to the neuraminidase (NA) protein as well as to HA because antibodies to NA are also protective and should thus affect clade fitness. We found large differences in the expected susceptibility of the population to different clades' HA and NA, and these differences in susceptibility predicted clade dominance. They also partially predicted the relative attack rates of clades by age. We furthermore quantified the heterogeneity in neutralizing titers in the population, finding patterns consistent with age-associated epitope targeting, despite a high diversity of neutralization profiles that gradually increases with age.

Results

Human sera from the summer of 2017 poorly neutralize the clade that dominated in North America in the next influenza season

We investigated whether neutralizing antibody titers to HA and NA from H3N2 clades circulating in early 2017 could predict the dominant (most frequent) clade in the next influenza season. Antibodies to HA can protect against infection [12, 13, 15–17], and we expected that the clade to which the largest fraction of the population had poorly neutralizing anti-HA titers would be most successful. This expectation assumes that exposure rates, other factors affecting susceptibility, and the average infectiousness or transmissibility of an infected person do not differ starkly between age groups; it also assumes that antibody-mediated protection derives primarily from neutralization and not Fc-mediated effector functions, or that the two are well correlated. Antibody neutralization was measured by the focus reduction neutralization test (FRNT). Correlates of protection have not been established for FRNT-derived titers, but because microneutralization titers correlate well with hemagglutination inhibition (HAI) [18], and a 1:40 HAI titer is traditionally associated with a 50% reduction in infection risk [12], we initially assumed a 1:40 FRNT titer corresponds to a 50% chance of infection, testing other assumptions in sensitivity analyses. We looked at the fraction of the population below this cutoff for each clade to obtain the expected relative susceptibility and ranked clades by this measure. We also estimated the relative susceptibility according to the geometric mean titer (GMT) to each clade, with lower GMT implying higher susceptibility. With both measures, the population-level susceptibility was estimated by weighting the susceptibility of different age groups according to their proportion in the population (Methods). We initially assumed 1:80 NA titer by the enzyme-linked lectin assay (ELLA) to be the 50% protective titer and later explored other assumptions.

We collected serum samples from May to August of 2017 from the University of Pennsylvania BioBank and Children's Hospital of Philadelphia [19] (Methods). Samples from children were primarily obtained for lead testing. Adults with certain health conditions were excluded. No information on vaccination status was available. We measured neutralizing titers to the 8 HA and 2 NA representing common current or recently circulating H3N2 clades (Fig 1A left for HA and Fig S1A left for NA).

The genetic diversity of the H3N2 HA was high in 2017. Two distinct clades, 3C.2A and 3C.3A, which last shared a common ancestor in 2012 circulated globally. These clades differed by amino acid substitutions in epitopes A and B (Fig 1B, C) and in non-epitope sites. Clade 3C.2A had gained a potential glycosylation site at epitope B (K160T; H3 numbering used throughout) and had lost a glycosylation motif at epitope A (N144S). Clade 3C.3A had lost a different glycosylation site in epitope A (T128A) (Fig 1B, C).

We picked at least one reference virus for each clade, further splitting clade 3C.2A into subclades 3C.2A1, 3C.2A2, and 3C.2A3. We chose as the reference virus for basal clade 3C.2A the H3N2 vaccine strain in the 2016-2017 season (A/Hong Kong/4801/2014). For subclades 3C.2A1, 3C.2A2, and 3C.2A3, we picked 3, 2, and 1 reference viruses, respectively, each carrying subclade-specific nonsynonymous substitutions and (for 3C.2A1 and 3C.2A2) potentially important amino acid polymorphisms within the subclade. Each subclade contained an epitope A substitution compared to the 3C.2A reference strain (Fig 1B, C). Notably, one reference virus for clade 3C.2A1 (virus 3C.2A1-3) had the T135K mutation, which removes a glycosylation motif in epitope A. For clade 3C.3A, we picked one reference virus.

For all reference viruses, an undetectable HA titer (titer of 1:10) was the most common HA titer in all age groups except children 5-17 years old (Figs 2A, S2). Most

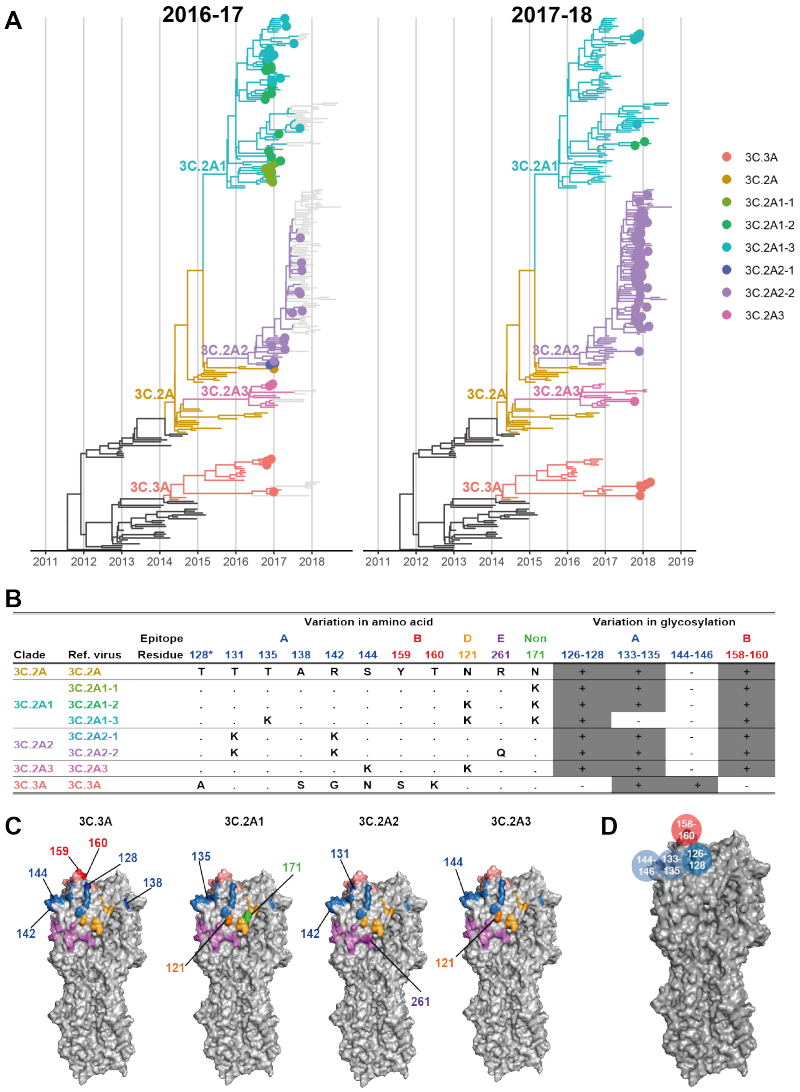

Fig 1. Reference viruses representing co-circulating H3N2 clades during the 2016-2017 season. A. Genealogies of H3N2 HA through the 2016-2017 (left) and 2017-2018 season (right). Branches are colored by clade. Tips are shown as filled circles if collected in North America during the most recent season. B. Amino acid and glycosylation site variation among reference viruses. Clades 3C.3A and 3C.2A diverge at additional non-epitope sites (not shown). Residue 128 belongs to antigenic site B, but the substitution T128A results in loss of glycosylation on residue 126 of epitope A. Therefore, we show residue 128 in epitope A and in the glycosylation site involving residues 126-128, following [1]. C. Variable residues among the reference viruses are shown on the H3 structure of A/Aichi/2/1968 (Protein Data Bank: 1HGG) and colored by epitope as in panel B. For each strain, residues differing from 3C.2A are numbered and darker in color. D. Glycosylation sites used in the model shown on the H3 structure.

people over 4 years old had detectable NA titers (1:$\geq$ 20) (Figs 3A, S3). Even though detectable antibody to H3N2 HA or NA is expected among older children and adults, who have been infected and possibly vaccinated with H3N2, surprisingly large variation was observed among individuals of the same age (Figs 2A, 3A). These are likely genuine

differences in titer, as technical replicates had high agreement.

The population-level relative susceptibility inferred using the 1:40 protective cutoff in HA titer was highest to the 3C.2A2 subclade, specifically the group of viruses with 261Q in epitope E (3C.2A2-2 reference strain; the susceptibility to 3C.2A2-2 is higher than the susceptibility to 3C.2A2-1 and 3C.3A, both bootstrap $p < 0.001$), followed by the rest of the 3C.2A2 subclade (3C.2A2-1 reference strain; the susceptibility to 3C.2A2-1 is higher than the susceptibility to 3C.2A1-1, bootstrap $p < 0.05$) and the 3C.3A clade ($p < 0.01$ for the same test; Fig 2B, left panel) (Methods). The GMTs also suggested the susceptibility was highest to the 3C.2A2-2 reference strain followed by 3C.2A2-1 (Fig S4). The greatest protection or lowest susceptibility in the population by both measures was to strains of the 3C.2A1 subclade with 135K in epitope A and 121K in epitope D (reference strain 3C.2A1-3) and subclade 3C.2A3 (reference strain 3C.2A3).

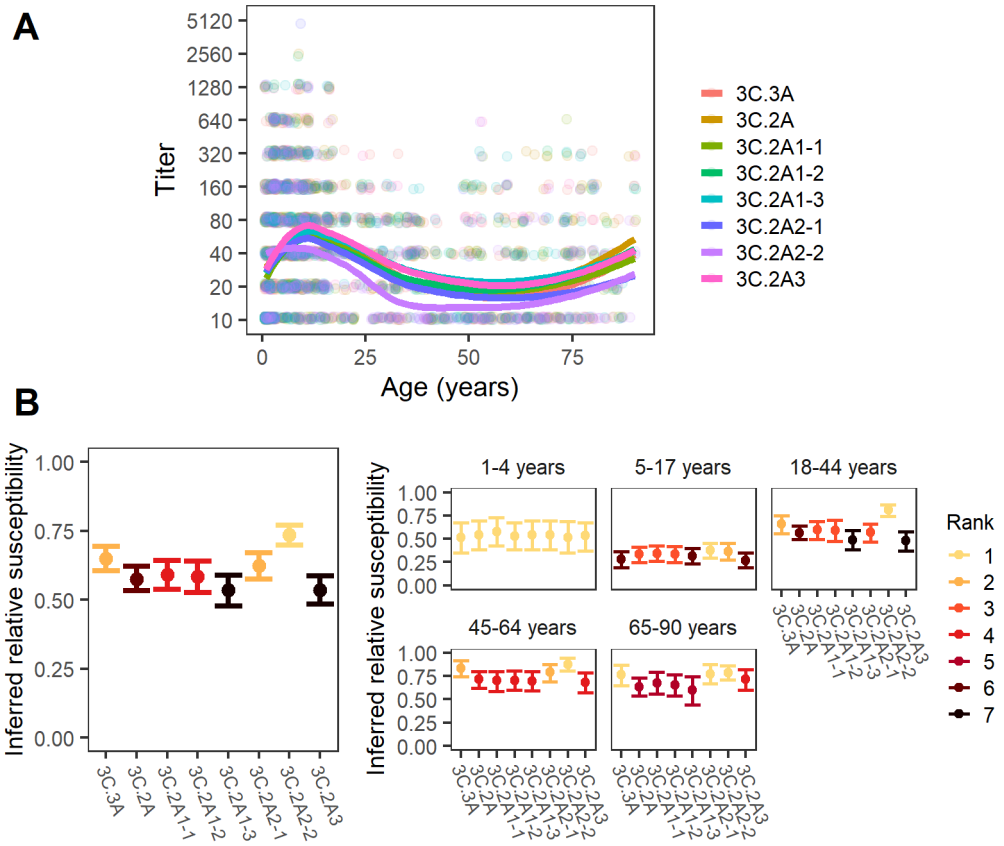

Fig 2. Antibody titers and inferred relative susceptibilities to co-circulating H3 strains show variability by strain and age group. A. FRNT titers with points jittered slightly along the x- and y-axes. Lines are Loess curves showing smoothed geometric mean titers. B. Inferred relative susceptibility and its rank to each reference strain for the whole population (left) and by age group (right). The bars indicate 95% CIs obtained from bootstrapping. A lower rank indicates significantly higher susceptibility.

Consistent with simple predictions, clade 3C.2A2 dominated in North America in the 2017-18 season (Fig 1A, right panel), followed by 3C.3A. To assess dominance, influenza sequences were downloaded from GISAID [20]. We assigned 9913 sequences collected in North America during the 2016-2017 and 2017-2018 influenza seasons to

reference viruses based on their genetic similarity at segregating sites and found that the frequency of sequences genetically similar to reference strain 3C.2A2-2 in clade 3C.2A2 increased from 21% in the 2016-2017 season to 85% in the 2017-2018 season (Fig S11). Clade 3C.3A increased from 6% to 8% over that period. However, we did not find a perfect correlation between the rank measured by inferred relative susceptibilities and rank by relative growth: despite having higher estimated susceptibility than subclade 3C.2A1 (3C.2A1-3), subclade 3C.2A1 (3C.2A1-2) experienced a more severe decline. Although the available sequences are not generated from any kind of systematic surveillance program and thus may not accurately reflect relative prevalence, trends were stable regionally (Fig S11A). The results suggest that population-average anti-HA neutralizing titers reflect strain fitness, but that other factors may be relevant for detailed predictions.

We next measured antibody responses to NA reference strains representing the NAs of clades 3C.2A and 3C.2A2 ("3C.2A (NA)" and "3C.2A2-2 (NA)", respectively) (Fig 3A) [19]. The two reference viruses differ by 7 amino acid substitutions in the NA head: 176, 245, 247, 329, 334, 339, and 386. We first estimated population-level relative susceptibilities to the two clades using a 1:80 protective cutoff (Fig 3B, left panel). Similar to our findings for HA, serological responses to NA indicated higher susceptibility to 3C.2A2-2 (NA) than to 3C.2A (NA) across all age groups. The GMT values also suggested higher susceptibility to 3C.2A2-2 (Figs 3A, S8). Because only two NA reference strains were used, we cannot conclude if anti-NA titers would have predicted clades' rank frequencies as accurately or perhaps better than titers to HA.

Age groups differ in their susceptibility to and relative attack rates with different H3N2 clades

Because age-specific patterns of antibody titers have been associated with age-specific infection risk [5, 21], we estimated relative susceptibility to each clade within each age group and measured correlations with their estimated relative clade-specific infection rates in the 2017-2018 influenza season. Age groups differed slightly in their expected susceptibilities to different clades of H3N2 (Fig 2B, right panel). Assessed by their anti-HA titers, children 1 to 4 years old appear equally susceptible to all reference viruses. The anti-HA titers of older children and adults showed heightened susceptibility to the 3C.2A2 clade: titers from 5- to 17-year-olds indicated the highest susceptibility to the basal 3C.2A2 clade (reference strain 3C.2A2-1) followed closely by 3C.2A2 (reference strain 3C.2A2-2), whereas people aged 18-64 y had pronounced susceptibility to reference strain 3C.2A2-2 compared to other clades. All age groups with previous influenza experience ($\geq$ 5 y) were least susceptible to clades 3C.2A1 and 3C.3A (reference strains 3C.2A1-3 and 3C.2A3, respectively). Interestingly, 5- to 17-year-olds were least susceptible to 3C.3A, while adults were relatively susceptible to 3C.3A. We also found that children 1 to 4 years old had comparable susceptibility to the two clades of NA, and all older age groups demonstrated greater susceptibility to the 3C.2A2 clade (3C.2A2-2 (NA)) (Fig 3B, right panel).

We evaluated whether the age-associated trends in relative susceptibilities to different clades in the summer of 2017 were mirrored in their relative rate of infection with each clade in the 2017-2018 influenza season. Due to lack of systematic surveillance, unbiased estimates of attack rates by clade do not exist for this population. We nonetheless examined the ages associated with sequences uploaded into GISAID to approximate the proportion of infections caused by each clade in each age group. Because the 3C.2A2 clade dominated in the 2017-2018 season and all but the youngest age groups showed particularly high susceptibility to this clade, we expected clade 3C.2A2 to be the most frequent within each age group. This is what we found (Fig S12).

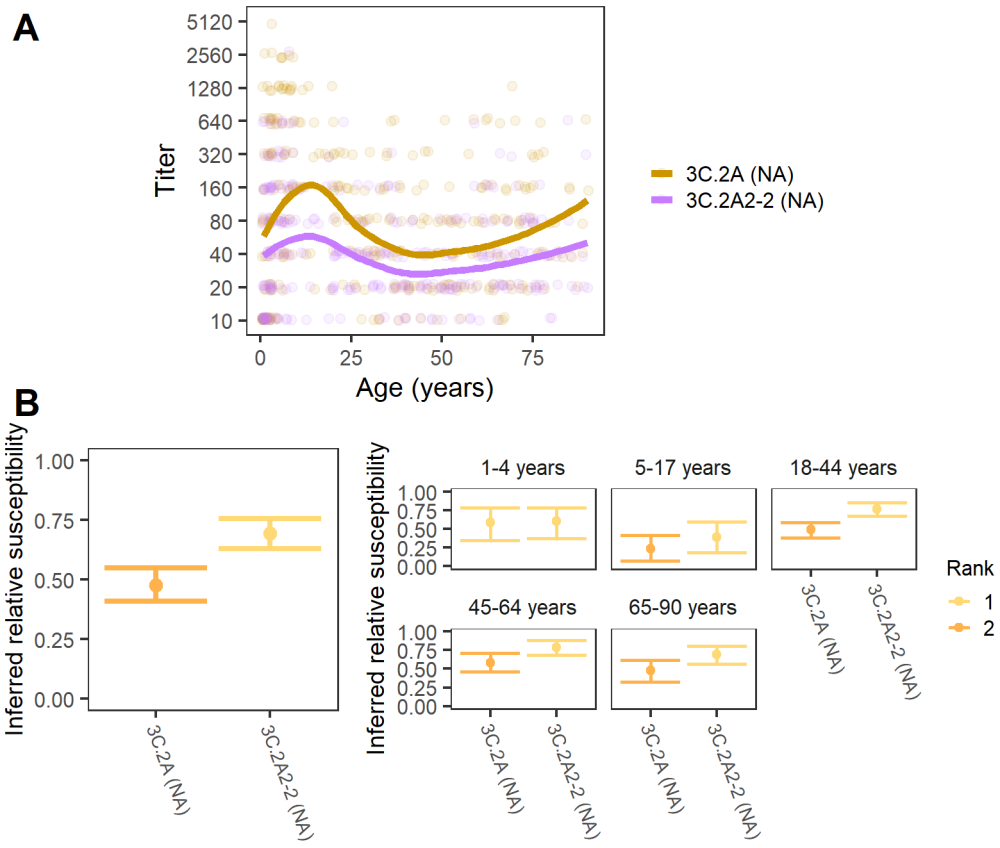

Fig 3. Antibody titers and relative susceptibilities to co-circulating N2 stains show differences by strain and age group. A. ELLA titers with points jittered slightly along the x- and y-axes. Lines are Loess curves showing smoothed geometric mean titers. B. Inferred relative susceptibility and its rank for each NA for the whole population (left) and by age group (right). A lower rank indicates significantly higher susceptibility.

However, we observed that children < 5 y old, who seemed approximately equally susceptible to all clades by HA and NA, had a relatively lower proportion of 3C.2A2 infections compared to adults (chi-square test, $p < 0.001$). Children 5-17 y old, who were only slightly more susceptible to 3C.2A2 than other clades, also had a lower proportion of 3C.2A2 infections compared to adults ($p < 0.001$). Consistent with our observation that 18- to 64-year-olds were disproportionately susceptible to clade 3C.2A2, the age distribution of that clade was slightly more skewed toward adults compared to non-3C.2A2 clades, which were more common in children (Fig S13).

Correlations between titers to different strains vary by age, suggesting age-associated differences in epitope targeting

We next investigated the correlations in titers to different clades (Fig 4A, blue lines): Do individuals with high titers to 3C.3A tend also to have high titers to 3C.2A2, for instance? Closely correlated titers to related viruses suggest that individuals might target epitopes conserved among them. (It could also indicate recent infections or immunizations with each of those strains and responses to their *non*-shared epitopes,

although H3N2 infections typically occur at least several years apart and are less frequent in adults compared to children [17, 22, 23].) Aside from providing insight into the mechanisms generating immunity, understanding the structure of titers within the population might lead to improved estimates of selective pressures on viruses. For instance, weakly correlated titers to different clades suggest a population with more heterogeneous immunity, which can affect viral coexistence, vaccination thresholds, and other dynamics [24–27].

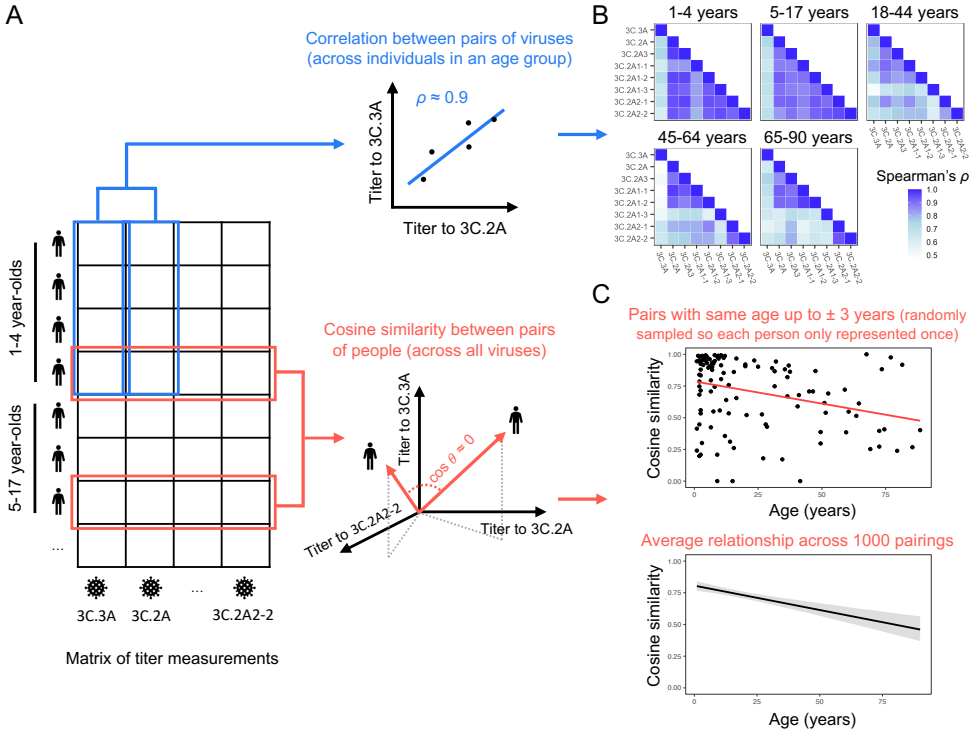

Fig 4. Correlations in titers to different clades and similarities of titer vectors of individuals A. Schematics demonstrating calculation of the correlation of titers to different strain pairs (within age groups; blue lines) and of the correlation between vectors of titers between pairs of individuals (cosine similarity; red lines). B. Correlations between titers to different strains differ by age group, suggesting age-dependent patterns of epitope targeting. Each cell is colored by the correlation coefficient for titers to that viral pair within that age group. Individuals with undetectable titers across all reference viruses have been removed. C. The similarity of titer vectors declines with age. In the upper panel, points show cosine similarities of HA titers between pairs of individuals. Each cosine similarity was calculated from a randomly drawn pair of individuals who were within a 3-year age difference. The regression line is shown in red. The lower panel shows the distribution of estimates obtained by regressing cosine similarity on age using 1000 different sets of random pairs. The black line is the mean of the predicted cosine similarity and the gray shading indicates the 95% interval of predicted values.

We found that the strength of correlation differed by age group and virus pair. In general, titers to all the reference viruses were highly correlated in 1- to 4-year-old children and less correlated in older ages (Figs 4B, S14). (Individuals with undetectable titers to all strains were removed from the main analysis.) This suggests that young children target epitopes common to many reference viruses or have been infected by

close relatives of each, whereas older age groups target epitopes conserved among only a subset (Figs S18, S19, S20). Results hold when age groups are chosen to span an equal number of years (Fig S15), showing that the weaker correlation in titers across all reference viruses in adults 18-44 y, 45-64 y, and 65-90 y is not due simply to the groups' relative sizes or the diversity of childhood exposures represented in them. In all age groups, titers to 3C.3A were least correlated with titers to other viruses (Fig S16). This might be explained by reduced exposure to 3C.3A viruses and/or the targeting of sites on 3C.2A clade viruses that are not shared with 3C.3A (Fig S17).

The strength of correlation between titers to 3C.2A clades varied between age groups. In contrast to younger age groups, middle-aged and older adults ($\geq$ 45 y) showed uniquely strong correlations in titers to 3C.2A, 3C.2A3 and 3C.2A1 with 135T (reference strains 3C.2A, 3C.2A3, 3C.2A1-1, and 3C.2A1-2). The pattern might be explained by responses focused on epitope A (e.g., sites 131, 135, and 142) residues that are disrupted in other reference strains.

Titer profiles or local antibody landscapes diversify with age

The prior analysis measured typical correlations between titers from the same individual to different reference strains and found that those correlations differed by age, suggesting that age groups vary in which sites they target. A distinct question is whether individuals tend to target the reference strains similarly, i.e., do individuals of the same age have consistently high and low titers to the same strains, and do these titer profiles (vectors) diverge or converge with age (Fig 4A, red lines)? This is analogous to measuring the diversity of antibody landscapes [28], although here we are looking at very recent H3N2 evolution. We excluded individuals with only undetectable titers (for which cosine similarity is undefined) and calculated the cosine similarity of randomly chosen pairs of people, requiring that members of the pair have a $\leq$ 3-year age difference. Cosine similarity declined gradually with age (linear regression, $p < 0.001$, Fig 4C, upper panel). The significance of this trend holds across different random pairings (Fig 4C, lower panel). The decline in cosine similarity suggests that antibody responses diversify with age: children start with relatively consistent patterns of epitope targeting, and individuals' patterns diverge over time. The result also holds when we combine all HA and NA strains in the titer vector (Fig S21).

Clustering suggests two general titer profiles

Given the high variance in titers within and between age groups, we next examined if there were more clearly distinguishable subpopulations that shared similar titer profiles (had high cosine similarity) to co-circulating viruses. We used k-means clustering to separate individuals by their FRNT titers to the eight HA reference strains. Clustering into two groups was best supported (Figs 5, S22). The first group has high titers to clade 3C.3A and low titers to clade 3C.2A viruses across all age groups. The second group shows similar titers to all viruses, with lowest titers to some 3C.2A2 strains (reference strain 3C.2A2-2) in adults. There was no mean age difference between the groups (mean age difference = 3.7 y, Pearson's test, $p = 0.44$), indicating that people who have higher titers to 3C.3A compared to 3C.2A exist across all age groups, and showing that age or birth year does not strongly predict relative titers to contemporaneous strains.

Relatively large differences in antibody titers to 3C.3A and 3C.2A strains are consistent with their sequence dissimilarity. Three potential N-linked glycosylation sites (PNGS) differ between 3C.3A and 3C.2A in epitopes A and B (Fig 1B): 3C.3A is missing a PNGS at sites 126-128 in epitope A and another at sites 158-160 in epitope B, whereas 3C.2A has no PNGS at sites 144-146 in epitope A. Epitope B is frequently

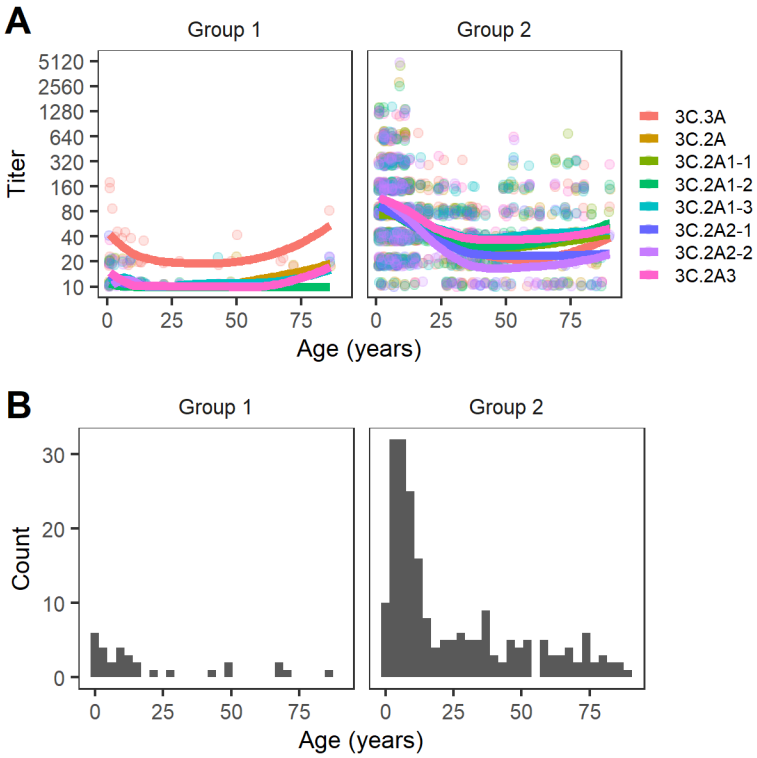

Fig 5. Individuals cluster into two groups by their vectors of HA titers or local antibody landscapes A. Titers of individuals in each group. Points are jittered slightly along the x- and y-axes. Lines are Loess curves showing smoothed geometric mean titers. B. The age distribution of each group.

immunodominant [29,30], and glycosylation at epitope B might shield some of the epitope [29]. Therefore, individuals with a high titer to 3C.3A relative to 3C.2A may have more antibodies directed toward epitope B. Alternatively or additionally, they may have epitope A immunodominance, and the PNGS at sites 126-128 in clade 3C.2A effectively shields the epitope.

Overall, the variance of differences in 3C.3A and 3C.2A log titers among individuals within an age group was as high as the variance among age groups (ANOVA, $F = 1.56$, $p = 0.18$), indicating factors other than age explain these coarse differences in specificity. However, the variance of differences between 3C.3A log titers and 3C.2A1-3, 3C.2A2-2, and 3C.2A3 log titers was more age-associated, although the results were not significant after correction for multiple tests (ANOVA, $p = 0.02$, 0.01, and 0.02, respectively; the cutoff for significance is 0.007 after Bonferroni correction; Table 1).

NA-focused antibody responses are more common in middle-aged adults

We next compared HA and NA antibody titers. The fraction of individuals with detectable HA titers decreased with age (Fig 6; logistic regression, $p < 0.01$; Methods). The fraction of people with titers only to NA increased with age (logistic regression, $p < 0.001$) and was highest among 51- to 60-y-olds, who were born between 1957 and 1966 (45% have NA only titers), followed by 41- to 50-y-olds, who were born between 1967 and 1976 (33% have NA only titers; Fig 6). This was the only period in which H1N1 did not circulate, and individuals in this age range were imprinted to or

Table 1. ANOVA test for whether the difference with 3C.3A log titers is higher among than within age groups

Ref. virus	Mean square (age group)	Mean square (residuals)	F	p
3C.2A	1.82	1.17	1.56	0.18
3C.2A1	3.14	1.41	2.22	0.07
3C.2A1-2	2.60	1.22	2.13	0.08
3C.2A1-3	4.16	1.47	2.84	0.02
3C.2A2	1.05	1.22	0.86	0.49
3C.2A2-2	5.15	1.41	3.64	0.01
3C.2A3	3.60	1.27	2.83	0.02

experienced original antigenic sin with the N2 NA through primary infection with H2N2 (which circulated from 1957-1968) or H3N2 (which circulated from 1968). We nonetheless find a positive correlation between individuals' HA and NA titers across all age groups, with a shift toward weaker correlations and higher NA than HA titers in older adults (Figs S23, S24).

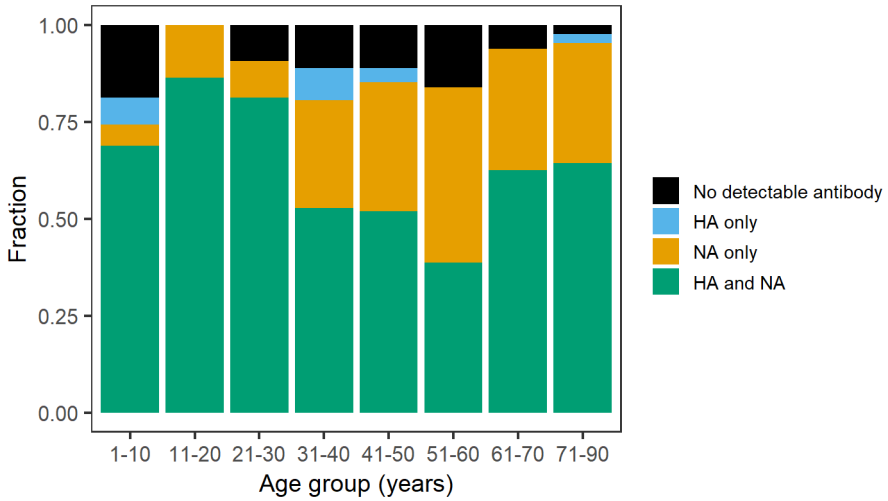

Fig 6. Antibody distributions for each age group. For both HA and NA, titers 1:$\geq$ 20 were defined as detectable antibody.

Discussion

Current approaches for forecasting influenza and mapping its antigenic evolution rely on antigenic distance measurements that do not always reflect immunity in the human population. Understanding the size of the difference and how much it matters would require analyzing discrepancies between antibody titers and traditional ferret-based measurements over multiple years from representative cross-sectional surveys in different populations. Multiple years of sampling could also resolve the subpopulations and measures needed to assess immune selective pressures and compare them to other factors influencing fitness [3, 31, 32]. Here, as a proof of principle, we demonstrate that several hundred sera obtained as convenience specimens from hospitals reveal differences in expected susceptibility to circulating HA clades that predict the clade circulating in

the following season. They also demonstrate high heterogeneity in neutralizing titers, which is partly age- and possibly birth-year-associated, and the consequences of which remain unclear.

The 2017-2018 influenza season in the United States was severe, causing approximately 41 million illnesses and 52,000 deaths [33]. The moderate effectiveness of the vaccine that season has been attributed to egg adaptations that created a mismatch to circulating strains [34]. The H3N2 component of the vaccine, A/Hong Kong/4801/2014 (a basal 3C.2A strain), had been unchanged from the previous season because no clear indication of antigenic evolution was apparent by early 2017, when vaccine strain composition for the Northern Hemisphere was decided; the 3C.2A2 clade was nonetheless noted to be growing quickly [35]. Over 90% of 3C.2A2 strains isolated from the United States in the 2017-2018 season were described as well inhibited by ferret antisera raised against the cell-propagated reference virus for A/Hong Kong/4801/2014 (A/Michigan/15/2014), and in early 2018, the H3N2 vaccine component was updated only to avoid egg adaptations, not because antigenic change had been detected [36]. (However, a later investigation of H3N2 viruses circulating in Japan in 2017-2018 did detect antigenic differences between 3C.2A and 3C.2A2 strains using ferret antisera [37].) Our study suggests that antigenic changes were detectable in human antisera by at least the summer of 2017, and they could predict the dominance of 3C.2A2. Consistent with this prediction, Ursin et al. found that individuals testing positive for H3N2 in the 2017-2018 season had consistently lower serum neutralization titers to the 3C.2A2 clade than those testing negative—with no differences between the two groups' titers to cell-grown A/Hong Kong/4801/2014—underscoring the consequences of these neutralization differences for protection and probably transmission [38].

Measurements of population immunity could be substantially more efficient and useful for forecasting if we understood exactly what to measure and in whom. Antibody titers to HA have been an established correlate of protection for half a century, and antibodies to NA for approximately a decade. The generally good concordance between hemagglutination inhibition assays and microneutralization suggest neutralization is a decent surrogate, but it is unclear how much protection each immune response confers in different people and whether measures of neutralization, total binding, antibody-dependent cellular cytoxicity or phagocytosis activity, and/or potentially other B- or T-cell or innate immune measures could improve estimates of relative susceptibility. Correlates likely vary in quality over time: large discrepancies between binding antibody titers and neutralization or protection have been reported and are likely associated with birth cohort [19, 39, 40]. Furthermore, an accurate evolutionary forecasting model would be grounded on correlates of transmission rather than simply protection against disease. It might also be important to weight immunity in different subpopulations differently: for instance, an infected child might be more likely to transmit than an infected adult. These considerations would affect the need to sample particular populations, such as unvaccinated members of certain age groups. Over larger geographic scales, samples from typical "source" populations may be better predictors or provide a longer lead time than populations that export fewer strains [41–43].

Our data revealed variation in antibody titers between age groups that are broadly consistent with influenza's epidemiology but lack precise explanation. Children over five years old had the highest geometric mean titers to all strains. This is consistent with the high attack rates in school-age children [44] and other studies that report young children having the high titers to recent strains [45]. Children also had relatively high vaccination coverage (approximately 59% in the 2016-2017 season in children $\geq$ 6 mos.) compared to younger adults [46]. These two factors might interact, since recent infection can boost vaccine immunogenicity [47, 48]. The relatively high vaccination coverage in the oldest age group (approximately 65% in adults $\geq$ 65 y) might explain

their higher titers compared to middle-aged and younger adults. Their relatively high titers might also be explained by a disproportionately NA-focused response among middle-aged adults whose likely first infections were with H2N2 between 1957 and 1968; most 40- to 60-year-old individuals had no detectable neutralizing antibodies to the HAs of circulating H3N2 clades. (These results suggest antibodies to HA may be a poor correlate of protection in this age group and complement other reports of their discrepant anti-HA titers [49].) Finally, we observed age-associated correlations in titers, with all strains except 3C.3A showing correlated titers in younger children but only a subset of 3C.2A strains (test strains 3C.2A3, 3C.2A1-1, 3C.2A1-2 and 3C.2A) showing correlated titers in older adults. This suggests differences in which epitopes are being targeted.

A prominent result, as in other seroepidemiological studies on influenza, is the large heterogeneity even within age groups [17, 28, 40, 45, 49, 50]. A clustering analysis suggested two major profiles of targeting, distinguished primarily by high vs. low titers to the 3C.3A clade, but these clusters are not strongly age-associated. Although not presented here, we fitted dozens of generalized linear mixed models to attempt to explain individuals' titers to these strains as a function of potential recent infections, vaccinations, early infections with strains with homologous epitopes, and individual-specific biases in the contributions of different epitopes to titers. These models were inconclusive, suggesting a need for more careful study of how a person's antibody titers change over time in response to particular exposures, and potentially with some deconvolution of the response to specific epitopes [51]. That repeated exposures might diversify responses was suggested by our discovery of a decline in the similarity of the vectors of titers with age.

Our results demonstrate the feasibility of detecting significant differences in neutralizing titers to different H3N2 clades in a sample of few hundred sera. This approach could entail substantial improvements over the use of ferret sera, which do not capture the immune history and heterogeneity in the human population. Testing improved sampling protocols and forecasting models, which would be facilitated by the existence of global blood banks [52, 53] and common standards [54], might yield rapid advances in forecasting not only the dominant clade but also potentially the dominant subtype, and ideally at longer lead times than shown here. If linked to other forms of surveillance, cross-sectional sera might also predict season severity and attack rates by age, as suggested here. The same samples and similar models might also predict the dynamics of other pathogens.

Materials and methods

Serological data

Sera from 489 individuals were collected between May and August of 2017 from the Children's Hospital of Philadelphia (1- to 17-year-olds) and from the University of Pennsylvania Health care system via Penn BioBank (18- to 90-y-olds), as reported om [19]. Serum samples were originally collected from children for lead testing, and leftover de-identified samples were then used for this study. The Penn BioBank routinely collects serum samples from individuals visiting the University of Pennsylvania Health care system. We did not include samples collected by the Penn BioBank from donors who had a pregnancy reported during the last 9 months, who had a medical history of cancer or organ transplantation, or who had a reported infectious disease within the previous 28 days. The study complied with all relevant ethical regulations and was approved by the Institutional Review Board of the University of Pennsylvania. Leftover de-identified samples collected at CHOP were considered exempt from human

research (exemption 4) since the samples were leftover discarded samples that were completely de-identified before our research team received them.

Foci reduction neutralization tests (FRNT) were performed on 437 individuals' sera using 8 viruses (3C.3A, 3C.2A, 3C.2A1-1, 3C.2A1-2, 3C.2A1-3, 3C.2A2-1, 3C.2A2-2 and 3C.2A3), and enzyme-linked lectin assays (ELLA) were performed on 352 individuals using NAs from two strains (3C2.A (NA) and 3C.2A2-2 (NA)) as described in [19]. HA and NA test virus used for 3C.2A is A/Colorado/15/2014, which is a reference virus for vaccine strain for the 2016-17 season and is used as a wild type strain to make viruses within 3C.2A. There were no significant titer differences between batches.

Genealogy of H3N2 and clade-specific amino acid substitutions

Prior to our analyses, we downloaded all available H3N2 HA and NA sequences from the 2012-13 season through the 2017-18 season from GISAID (accessed in 01/10/2022). Sequences were aligned using MAFFT 7.310 [55].

We downsampled sequences to construct the phylogeny. From the 2012-13 through the 2015-16 season, we sampled 20 sequences per season. For the 2016-17 and 2017-18 season, 100 sequences were sampled per season. The GISAID accession IDs and metadata of the sequences used for the analysis are available in the Supporting Information. We used BEAST 2.6.6 to reconstruct the genealogy [56] with a HKY substitution model [57] with a four-category gamma site model with 4 and a log normal relaxed clock. A coalescent Bayesian Skyline tree was used for the prior. We ran the chain for 50 million steps and saved every 1000 trees, using 5 million steps as burn-in. The maximum clade credibility tree was obtained using TreeAnnotator 2.6.6 version.

To visualize the tree, we used the R package ggtree 3.0.4 [58]. The trees were colored by clade. For the genealogy of the 2016-17 season, only tips of sequences collected in North America during the 2016-17 season were shown; these circled tips are colored according to their assigned clade. For sequences collected in other areas or seasons, only branches were shown. Similarly, for the genealogy of the 2017-18 season, only sequences collected in North America in that season are shown as colored circles.

Sequence samples were assigned to reference viruses according to reference virus-specific mutations at segregating sites, shown in Fig 1B. Here, sequences were assigned to each reference virus rather than the subclade represented by each reference strain. This is because sequences with 171K, 121K, and 135K, such as reference strain 3C.2A1-3, occur multiple times in clade 3C.2A1, and thus these sequences do not belong to any one subclade of 3C.2A1. Additionally, within a subclade, mutations at segregating sites occur so that a sequence in the same clade as a reference virus may not share the same genetic characteristics. Due to frequent mutation at residue 142 across most of clades, we allowed residue 142 to have any amino acid across most of clades, except for clade 3C.2A2, which has a clade-specific 142K substitution. We confirmed that all the sequences assigned to a reference virus fall in the same subclade as the reference virus.

Clade-specific substitutions were colored by epitope on the H3 structure using PyMOL version 2.3.3 [59].

Inferring relative susceptibility from titers

The "inferred relative susceptibility" to a strain equals the fraction of an age group's titers to that strain under some threshold (here, initially 40 for HA and 80 for NA), weighted by the fraction of the U.S. population projected to be in that age group in 2017 [60]. When there were fewer than eight titer measurements for a year of age, that age was grouped with the next year of age until the age group contained at least eight titer measurements. We found that using alternate titer thresholds for HA (Figs S5, S6,

and S7) and NA (Figs S9 and S10) resulted in consistent relative susceptibilities across strains.

The relative susceptibility was alternatively measured by the geometric mean titer (GMT). The GMT was weighted analogously by the population fraction of each age bin. Because lower GMTs correspond to higher susceptibility, we used a reverse scale when showing the relative susceptibility by GMT.

To test for meaningful differences in relative susceptibilities, we bootstrapped individuals to determine if the difference in inferred relative susceptibilities between two viruses was significantly greater than zero [61]. For each age bin, individuals were resampled 1000 times with replacement, and the fraction of individuals susceptible to each virus was calculated. For a given pair of viruses, we defined the relative susceptibility difference observed in the data as $\hat{\theta}$. The bootstrap value of $\hat{\theta}$, $\hat{\theta}^*$, was obtained 1000 times by resampling individuals. Then we obtained the null distribution of $(\hat{\theta}^* - \hat{\theta})$ and calculated the probability (p) of observing $\hat{\theta}$ or a greater value under this null distribution. If $p < 0.05$, the relative susceptibility difference is significantly greater than zero, i.e., susceptibility to the first virus significantly exceeded that to the second virus. For a given virus, we perform this comparison against all other viruses and counted the number of significant results. The more significant results, the lower the rank (closer to 1) of the relative susceptibility to a virus. We used the same approach and significance level for all other bootstrapping analyses.

Frequencies of subclades

To calculate the frequencies of different subclades in the 2016-17 and 2017-18 seasons, we downloaded sequences from GISAID on January 10, 2022, and assigned sequences to each subclade using the same method as was used to construct the genealogy. Because there were few sequences from Philadelphia, we calculated subclade frequencies in three different ways, using sequences collected from North America, United States, or the northeastern US. We considered Region 1, Region 2, and Region 3 of the U.S. Outpatient Influenza-like Illness Surveillance Network (ILINet, [46]) as the Northeastern U.S. states. These states are Connecticut, Maine, Massachusetts, New Hampshire, Rhode Island, Vermont, New Jersey, New York, Delaware, the District of Columbia, Maryland, Pennsylvania, Virginia, and West Virginia. Region 2 of ILINet includes Puerto Rico and the Virgin Islands, but we excluded them from the analysis of the northeastern U.S. For estimates derived from North American sequences, we used 4488 and 5425 sequences from the 2016-17 and 2017-18 seasons, respectively. For the US, 3707 and 3782 sequences were used. For the northeastern US, 782 and 676 sequences were used. The GISAID accession IDs and metadata of the sequences used for the analysis are available in the Supporting Information.

Correlations between titers to different strains

For each age group and pair of viruses, we calculated Spearman's ρ using the cor function in R. For each virus pair, we tested the difference in correlation coefficients between the youngest age group and each other age group by bootstrapping (Fig S14).

We also used bootstrapping to evaluate differences in correlation coefficients between viral pairs within an age group. For each virus pair, we did a series of bootstrap tests comparing the pair's correlation coefficient with the coefficient for each of the other pairs. Then, for each virus pair, the number of tests in which the pair's correlation was significantly weaker than that of other pairs within the group was counted. In each age group, there are 28 virus pairs whose correlation coefficient was calculated. One of the pairs, for example, is 3C.3A and 3C.2A, and this pair's correlation coefficient is compared with the other 27 correlation coefficients of other virus pairs. The 3C.3A v.

3C.2A pair's correlation was weaker than 15 other pairs' correlations. This number of tests in which the pair's correlation was significantly weaker than other pairs within the group is shown as the color intensity of the heat map of Fig S16.

Cosine similarities

To calculate the cosine similarities of titer vectors between pairs of individuals, we randomly drew pairs with a $\leq$ 3-year age difference. We sampled the pairs such that each person was represented only once (so the pairs would be statistically independent). Individuals with undetectable titers to all strains or with any missing data were removed from the analysis, because cosine similarity for such individuals cannot be defined. There were 244 individuals for analysis of HA titer vectors. For analysis of HA-NA titer vectors, there were 241 individuals, because HA and NA data were not available for all participants. Ultimately, there were 120 pairs for the HA titer vector analysis and 117 pairs for the HA-NA vector analysis. A pair's age was defined as the average age of the two individuals. Linear regression was performed to regress cosine similarity on age using the lm function in R. We repeated this analysis by randomly sampling pairs 1000 times to confirm that the trend by age is not caused by a particular pairing. For each set of sampled pairs, we recorded the slopes and predicted values. From this record, the mean and 95% interval of predicted values for each age year were calculated to show the distribution of the trend by age.

Clustering of individuals using titers

We used k-means clustering to partition individuals using their HA titers. For each individual, a vector of $\log_2$ titers was normalized and used as input for clustering based on cosine similarity. Vectors with all 0 (undetectable titers) were removed as their cosine similarity is undefinable. The CascadeKM function of the R vegan package was used with the Calinski-Harabasz criterion and the number of iterations set to 1500.

To test whether the between-group variance of differences in 3C.3A log titer and other reference viruses' log titers exceeded the within-group variance, we performed ANOVA. We first calculated differences between 3C.3A log titers and each of other reference viruses' log titers for each individual. Then we used the aov function in R 4.1.1 to perform ANOVA to test difference in the mean of the log titer differences among age groups.

The fraction of individuals with detectable HA or NA antibody

An individual was determined to have detectable HA antibody if there was at least one detectable HA titer to HA reference viruses (3C.3A, 3C.2A, 3C.2A1-1, 3C.2A1-2, 3C.2A1-3, 3C.2A2-1, 3C.2A2-2, and 3C.2A3). An individual was determined to have detectable NA antibody if there was at least one detectable titer to a NA reference virus (3C.2A (NA) and 3C.2A2 (NA)). For both HA and NA, titers $\geq$ 20 were defined as detectable.

We performed logistic regression using the glm function in R to test if the fraction of individuals with detectable HA antibody, detectable NA antibody, detectable HA antibody (only), and detectable NA antibody (only) changes with age.

Acknowledgments

We thank Ed Baskerville for extensive help with analytic models that were ultimately not included in this paper but shaped the direction of the work. We thank Manon Ragonnet-Cronin and Jesse Bloom for comments on the manuscript. We gratefully acknowledge all GISAID data contributors, i.e., the authors and their originating laboratories responsible for obtaining the specimens, and their submitting laboratories for generating the genetic sequence and metadata and sharing via the GISAID Initiative, on which this research is based.

Author contributions

Conceptualization–SC, SH. Formal analysis–KK, MCV, SC. Investigation–SG, MW. Supervision–SC, SH. Writing, original draft preparation–KK, MCV, SC. Writing, review and editing–KK, MCV, SG, SH, SC.

Competing interests

The authors declare they have no competing interests.

Funding

This project has been funded in part with Federal funds from the National Institute of Allergy and Infectious Diseases, National Institutes of Health, Department of Health and Human Services under CEIRS contract HHSN272201400005C (to SC) and CEIRR contract 75N93021C00015 to SC and SH and 1R01AI108686 to SH. The content is solely the responsibility of the authors and does not necessarily represent the official views of the NIAID or the National Institutes of Health.

Data and software availability

All data and code used in this analysis are available at `https://github.com/cobeylab/population_immunity_predicting_flu.git`. The Sequences obtained from GISAID and used for the analyses can be accessed using the accession IDs provided in Supporting information.

References

1. Jorquera PA, Mishin VP, Chesnokov A, Nguyen HT, Mann B, Garten R, et al. Insights into the antigenic advancement of influenza A (H3N2) viruses, 2011–2018. Scientific reports. 2019;9(1):1–16.
2. McCauley J, Daniels R, Lin Y, Xiang Z, Gregory V, Whittaker L, et al. Report prepared for the WHO Annual Consultation on the Composition of Influenza Vaccine for the Northern Hemisphere 2017-2018. The Crick Worldwide Influenza Centre (WIC), WHO CC for Reference & Research on Influenza. 2017;.
3. Huddleston J, Barnes JR, Rowe T, Xu X, Kondor R, Wentworth DE, et al. Integrating genotypes and phenotypes improves long-term forecasts of seasonal influenza A/H3N2 evolution. eLife. 2020;9. doi:10.7554/elife.60067.

4. Wentworth DE. Vaccines and Related Biological Products Advisory Committee October 6, 2022 Meeting Presentation—Global Influenza Virus Surveillance and Characterization; 2022. Available from: https://www.fda.gov/media/162115/download.

5. Linderman SL, Chambers BS, Zost SJ, Parkhouse K, Li Y, Herrmann C, et al. Potential antigenic explanation for atypical H1N1 infections among middle-aged adults during the 2013–2014 influenza season. Proceedings of the National Academy of Sciences. 2014;111(44):15798–15803.

6. Cobey S, Gouma S, Parkhouse K, Chambers BS, Ertl HC, Schmader KE, et al. Poor Immunogenicity, Not Vaccine Strain Egg Adaptation, May Explain the Low H3N2 Influenza Vaccine Effectiveness in 2012–2013. Clinical Infectious Diseases. 2018;67(3):327–333. doi:10.1093/cid/ciy097.

7. Fonville JM, Fraaij PLA, de Mutsert G, Wilks SH, van Beek R, Fouchier RAM, et al. Antigenic Maps of Influenza A(H3N2) Produced With Human Antisera Obtained After Primary Infection. Journal of Infectious Diseases. 2015;213(1):31–38. doi:10.1093/infdis/jiv367.

8. Davenport FM, Hennessy AV, Francis Jr T. Epidemiologic and immunologic significance of age distribution of antibody to antigenic variants of influenza virus. The Journal of experimental medicine. 1953;98(6):641–656.

9. Francis T, Davenport F, Hennessy A. A serological recapitulation of human infection with different strains of influenza virus. Transactions of the Association of American Physicians. 1953;66:231–239.

10. de St Groth SF, Webster R. Disquisitions on original antigenic sin: I. Evidence in man. The Journal of experimental medicine. 1966;124(3):331–345.

11. Li Y, Myers JL, Bostick DL, Sullivan CB, Madara J, Linderman SL, et al. Immune history shapes specificity of pandemic H1N1 influenza antibody responses. Journal of Experimental Medicine. 2013;210(8):1493–1500.

12. Hobson D, Curry R, Beare A, Ward-Gardner A. The role of serum haemagglutination-inhibiting antibody in protection against challenge infection with influenza A2 and B viruses. Epidemiology & Infection. 1972;70(4):767–777.

13. Tsang TK, Cauchemez S, Perera RA, Freeman G, Fang VJ, Ip DK, et al. Association between antibody titers and protection against influenza virus infection within households. The Journal of infectious diseases. 2014;210(5):684–692.

14. Monto AS, Petrie JG, Cross RT, Johnson E, Liu M, Zhong W, et al. Antibody to influenza virus neuraminidase: an independent correlate of protection. The Journal of infectious diseases. 2015;212(8):1191–1199.

15. Ng S, Nachbagauer R, Balmaseda A, Stadlbauer D, Ojeda S, Patel M, et al. Novel correlates of protection against pandemic H1N1 influenza A virus infection. Nature medicine. 2019;25(6):962–967.

16. Cowling BJ, Lim WW, Perera RAPM, Fang VJ, Leung GM, Peiris JSM, et al. Influenza Hemagglutination-inhibition Antibody Titer as a Mediator of Vaccine-induced Protection for Influenza B. Clinical Infectious Diseases. 2018;68(10):1713–1717. doi:10.1093/cid/ciy759.

17. Ranjeva S, Subramanian R, Fang VJ, Leung GM, Ip DKM, Perera RAPM, et al. Age-specific differences in the dynamics of protective immunity to influenza. Nature Communications. 2019;10(1). doi:10.1038/s41467-019-09652-6.

18. Verschoor CP, Singh P, Russell ML, Bowdish DME, Brewer A, Cyr L, et al. Microneutralization Assay Titres Correlate with Protection against Seasonal Influenza H1N1 and H3N2 in Children. PLOS ONE. 2015;10(6):e0131531. doi:10.1371/journal.pone.0131531.

19. Gouma S, Kim K, Weirick ME, Gumina ME, Branche A, Topham DJ, et al. Middle-aged individuals may be in a perpetual state of H3N2 influenza virus susceptibility. Nature communications. 2020;11(1):1–8.

20. Elbe S, Buckland-Merrett G. Data, disease and diplomacy: GISAID's innovative contribution to global health. Global Challenges. 2017;1(1):33–46. doi:10.1002/gch2.1018.

21. Huang KYA, Rijal P, Schimanski L, Powell TJ, Lin TY, McCauley JW, et al. Focused antibody response to influenza linked to antigenic drift. Journal of Clinical Investigation. 2015;125(7):2631–2645. doi:10.1172/jci81104.

22. Kucharski AJ, Lessler J, Read JM, Zhu H, Jiang CQ, Guan Y, et al. Estimating the Life Course of Influenza A(H3N2) Antibody Responses from Cross-Sectional Data. PLOS Biology. 2015;13(3):e1002082. doi:10.1371/journal.pbio.1002082.

23. Kucharski AJ, Lessler J, Cummings DAT, Riley S. Timescales of influenza A/H3N2 antibody dynamics. PLOS Biology. 2018;16(8):e2004974. doi:10.1371/journal.pbio.2004974.

24. Cobey S, Pascual M. Consequences of host heterogeneity, epitope immunodominance, and immune breadth for strain competition. Journal of Theoretical Biology. 2011;270(1):80–87. doi:10.1016/j.jtbi.2010.11.009.

25. Zinder D, Bedford T, Gupta S, Pascual M. The Roles of Competition and Mutation in Shaping Antigenic and Genetic Diversity in Influenza. PLoS Pathogens. 2013;9(1):e1003104. doi:10.1371/journal.ppat.1003104.

26. Marchi J, Lässig M, Walczak AM, Mora T. Antigenic waves of virus–immune coevolution. Proceedings of the National Academy of Sciences. 2021;118(27). doi:10.1073/pnas.2103398118.

27. Makau DN, Lycett S, Michalska-Smith M, Paploski IAD, Cheeran MCJ, Craft ME, et al. Ecological and evolutionary dynamics of multi-strain RNA viruses. Nature Ecology & Evolution. 2022;6(10):1414–1422. doi:10.1038/s41559-022-01860-6.

28. Fonville J, Wilks S, James S, Fox A, Ventresca M, Aban M, et al. Antibody landscapes after influenza virus infection or vaccination. Science. 2014;346(6212):996–1000.

29. Zost SJ, Parkhouse K, Gumina ME, Kim K, Perez SD, Wilson PC, et al. Contemporary H3N2 influenza viruses have a glycosylation site that alters binding of antibodies elicited by egg-adapted vaccine strains. Proceedings of the National Academy of Sciences. 2017;114(47):12578–12583.

30. Lee JM, Eguia R, Zost SJ, Choudhary S, Wilson PC, Bedford T, et al. Mapping person-to-person variation in viral mutations that escape polyclonal serum targeting influenza hemagglutinin. Elife. 2019;8.

31. Powell H, Pekosz A. Neuraminidase antigenic drift of H3N2 clade 3c.2a viruses alters virus replication, enzymatic activity and inhibitory antibody binding. PLOS Pathogens. 2020;16(6):e1008411. doi:10.1371/journal.ppat.1008411.

32. Liu T, Wang Y, Tan TJC, Wu NC, Brooke CB. The evolutionary potential of influenza A virus hemagglutinin is highly constrained by epistatic interactions with neuraminidase. Cell Host & Microbe. 2022;30(10):1363–1369.e4. doi:10.1016/j.chom.2022.09.003.

33. Centers for Disease Control and Prevention. Estimated Flu-Related Illnesses, Medical Visits, Hospitalizations, and Deaths in the United States — 2017–2018 Flu Season; 2021. Available from: `https://archive.cdc.gov/#/details?url=https://www.cdc.gov/flu/about/burden/2017-2018.htm`.

34. Rolfes MA, Flannery B, Chung JR, O'Halloran A, Garg S, Belongia EA, et al. Effects of Influenza Vaccination in the United States During the 2017–2018 Influenza Season. Clinical Infectious Diseases. 2019;69(11):1845–1853. doi:10.1093/cid/ciz075.

35. Bedford T, Neher RA. Seasonal influenza circulation patterns and projections for 2017-2018. bioRxiv. 2017;doi:10.1101/113035.

36. Garten R, Blanton L, Elal AIA, Alabi N, Barnes J, Biggerstaff M, et al. Update: Influenza Activity in the United States During the 2017–18 Season and Composition of the 2018–19 Influenza Vaccine. MMWR Morbidity and Mortality Weekly Report. 2018;67(22):634–642. doi:10.15585/mmwr.mm6722a4.

37. Kawakami C, Yamayoshi S, Akimoto M, Nakamura K, Miura H, Fujisaki S, et al. Genetic and antigenic characterisation of influenza A(H3N2) viruses isolated in Yokohama during the 2016/17 and 2017/18 influenza seasons. Eurosurveillance. 2019;24(6). doi:10.2807/1560-7917.es.2019.24.6.1800467.

38. Ursin RL, Liu H, Powell HR, Westerbeck JW, Shaw-Saliba K, Sylvia KE, et al. Differential Antibody Recognition of H3N2 Vaccine and Seasonal Influenza Virus Strains Based on Age, Vaccine Status, and Sex in the 2017–2018 Season. The Journal of Infectious Diseases. 2020;222(8):1371–1382. doi:10.1093/infdis/jiaa289.

39. Arevalo CP, Sage VL, Bolton MJ, Eilola T, Jones JE, Kormuth KA, et al. Original antigenic sin priming of influenza virus hemagglutinin stalk antibodies. Proceedings of the National Academy of Sciences. 2020;117(29):17221–17227. doi:10.1073/pnas.1920321117.

40. Yang B, García-Carreras B, Lessler J, Read JM, Zhu H, Metcalf CJE, et al. Long term intrinsic cycling in human life course antibody responses to influenza A(H3N2): an observational and modeling study. eLife. 2022;11. doi:10.7554/elife.81457.

41. Lemey P, Rambaut A, Bedford T, Faria N, Bielejec F, Baele G, et al. Unifying Viral Genetics and Human Transportation Data to Predict the Global Transmission Dynamics of Human Influenza H3N2. PLoS Pathogens. 2014;10(2):e1003932. doi:10.1371/journal.ppat.1003932.

42. Bahl J, Nelson MI, Chan KH, Chen R, Vijaykrishna D, Halpin RA, et al. Temporally structured metapopulation dynamics and persistence of influenza A H3N2 virus in humans. Proceedings of the National Academy of Sciences. 2011;108(48):19359–19364. doi:10.1073/pnas.1109314108.

43. Russell CA, Jones TC, Barr IG, Cox NJ, Garten RJ, Gregory V, et al. The Global Circulation of Seasonal Influenza A (H3N2) Viruses. Science. 2008;320(5874):340–346. doi:10.1126/science.1154137.

44. Arevalo P, McLean HQ, Belongia EA, Cobey S. Earliest infections predict the age distribution of seasonal influenza A cases. Elife. 2020;9:e50060.

45. Lessler J, Riley S, Read JM, Wang S, Zhu H, Smith GJ, et al. Evidence for antigenic seniority in influenza A (H3N2) antibody responses in southern China. PLoS pathogens. 2012;8(7).

46. Centers for Disease Control and Prevention. FluVaxView; 2023. Available from: `https://www.cdc.gov/flu/fluvaxview/1516season.htm`.

47. Auladell M, Phuong HVM, Mai LTQ, Tseng YY, Carolan L, Wilks S, et al. Influenza virus infection history shapes antibody responses to influenza vaccination. Nature Medicine. 2022;28(2):363–372. doi:10.1038/s41591-022-01690-w.

48. Krammer F, Srivastava K, Alshammary H, Amoako AA, Awawda MH, Beach KF, et al. Antibody Responses in Seropositive Persons after a Single Dose of SARS-CoV-2 mRNA Vaccine. New England Journal of Medicine. 2021;384(14):1372–1374. doi:10.1056/nejmc2101667.

49. Vinh DN, Nhat NTD, de Bruin E, Vy NHT, Thao TTN, Phuong HT, et al. Age-seroprevalence curves for the multi-strain structure of influenza A virus. Nature Communications. 2021;12(1). doi:10.1038/s41467-021-26948-8.

50. Edler P, Schwab LSU, Aban M, Wille M, Spirason N, Deng YM, et al. Differential cross-reactivity to the influenza B virus haemagglutinin underpins lineage-specific susceptibility between birth cohorts. bioRxiv. 2023;doi:10.1101/2023.08.25.554879.

51. Einav T, Creanga A, Andrews SF, McDermott AB, Kanekiyo M. Harnessing low dimensionality to visualize the antibody–virus landscape for influenza. Nature Computational Science. 2022;3(2):164–173. doi:10.1038/s43588-022-00375-1.

52. Metcalf CJE, Farrar J, Cutts FT, Basta NE, Graham AL, Lessler J, et al. Use of serological surveys to generate key insights into the changing global landscape of infectious disease. The Lancet. 2016;388(10045):728–730. doi:10.1016/s0140-6736(16)30164-7.

53. Mina MJ, Metcalf CJE, McDermott AB, Douek DC, Farrar J, Grenfell BT. A Global lmmunological Observatory to meet a time of pandemics. eLife. 2020;9. doi:10.7554/elife.58989.

54. Horby PW, Laurie KL, Cowling BJ, Engelhardt OG, Sturm-Ramirez K, Sanchez JL, et al. CONSISE statement on the reporting of Seroepidemiologic Studies for influenza (ROSES-I statement): an extension of the STROBE statement. Influenza and Other Respiratory Viruses. 2016;11(1):2–14. doi:10.1111/irv.12411.

55. Katoh K, Misawa K, Kuma Ki, Miyata T. MAFFT: a novel method for rapid multiple sequence alignment based on fast Fourier transform. Nucleic acids research. 2002;30(14):3059–3066.

56. Bouckaert R, Heled J, Kühnert D, Vaughan T, Wu CH, Xie D, et al. BEAST 2: a software platform for Bayesian evolutionary analysis. PLoS computational biology. 2014;10(4).

57. Hasegawa M, Kishino H, Yano Ta. Dating of the human-ape splitting by a molecular clock of mitochondrial DNA. Journal of molecular evolution. 1985;22(2):160–174.

58. Yu G, Smith DK, Zhu H, Guan Y, Lam TTY. ggtree: an R package for visualization and annotation of phylogenetic trees with their covariates and other associated data. Methods in Ecology and Evolution. 2017;8(1):28–36.

59. Schrödinger, LLC. The PyMOL Molecular Graphics System, Version 2.0;. Available from: `https://pymol.org/2/`.

60. Colby SL, Ortman JM. Projections of the Size and Composition of the US Population: 2014 to 2060. Population Estimates and Projections. Current Population Reports. P25-1143. US Census Bureau. 2015;.

61. Hall P, Wilson SR. Two guidelines for bootstrap hypothesis testing. Biometrics. 1991; p. 757–762.

Supporting information

S1 File. GISAID Acknowledge table

S2 File GISAID accession IDs and metadata of the sequences used for constructing genealogy

S3 File GISAID accession IDs and metadata of the sequences used in the analysis of subclade frequency

Supplementary Figures

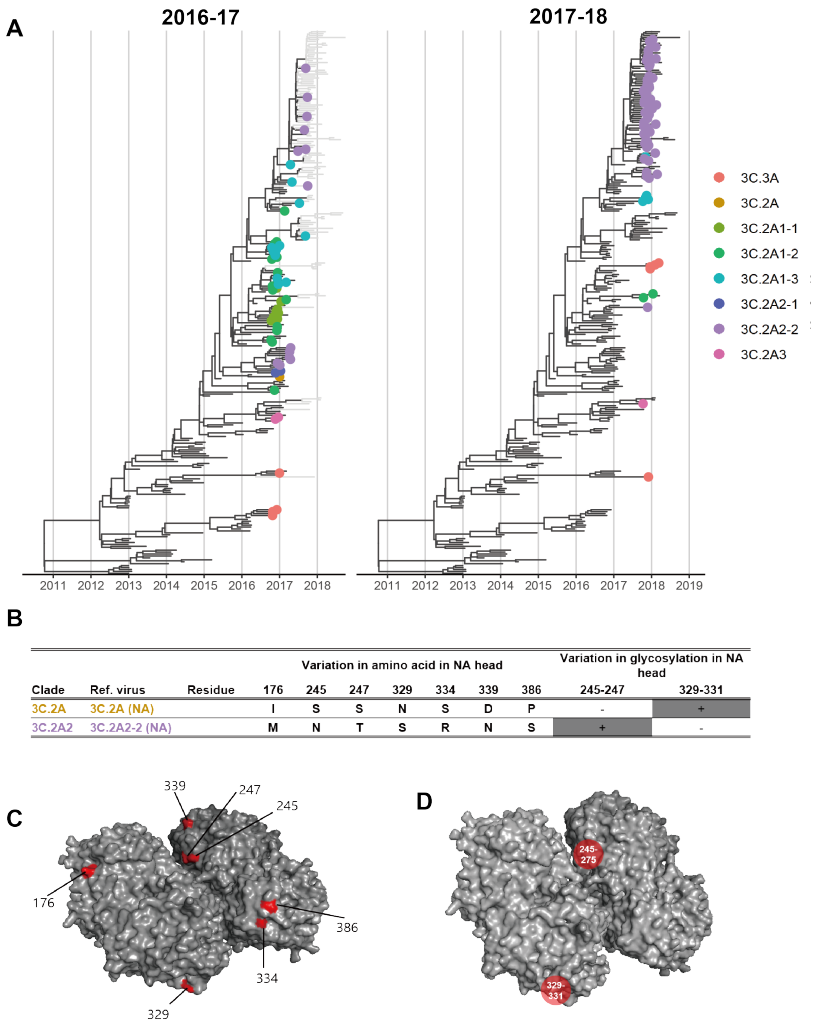

Fig S1. NA of co-circulating H3N2 clades during the 2016-17 and 2017-18 seasons. A. Genealogy of H3N2 showing NA sequence samples through the 2016-17 season (left) and through the 2017-18 season (right). Tips are filled circles if collected in North America during the 2016-17 season (left) and the 2017-18 season (right) and colored according to the associated test virus. B. Variable amino acids and PNGS between test viruses. Between clade 3C.2A (NA)and clade 3C.2A2 (NA), only substitutions at NA head are shown. C. The differences between clade 3C.2A (NA) and 3C.2A2-2 (NA) are shown on N2 head structure (Protein Data Bank: 6n4d). Amino acid differences between the two test viruses are colored in red. D. PNGS that vary between 3C.2A (NA) and 3C.2A2 (NA) are shown on the N2 structure.

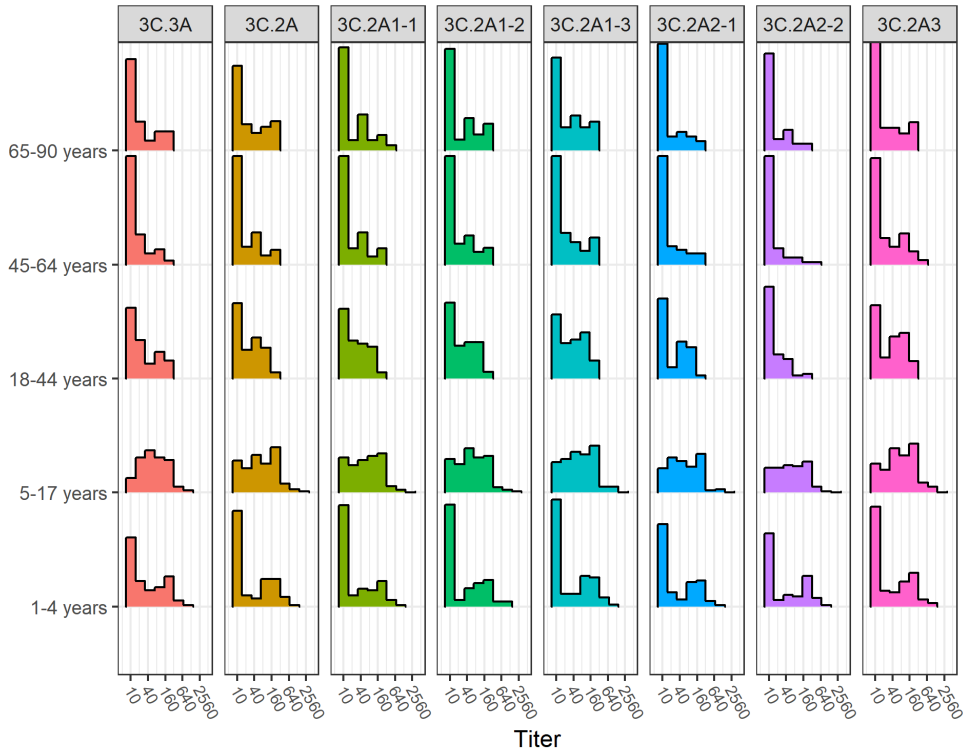

Fig S2. Distribution of HA titers for each strain by age group. A titer of 10 indicates the titer is below the limit of detection.

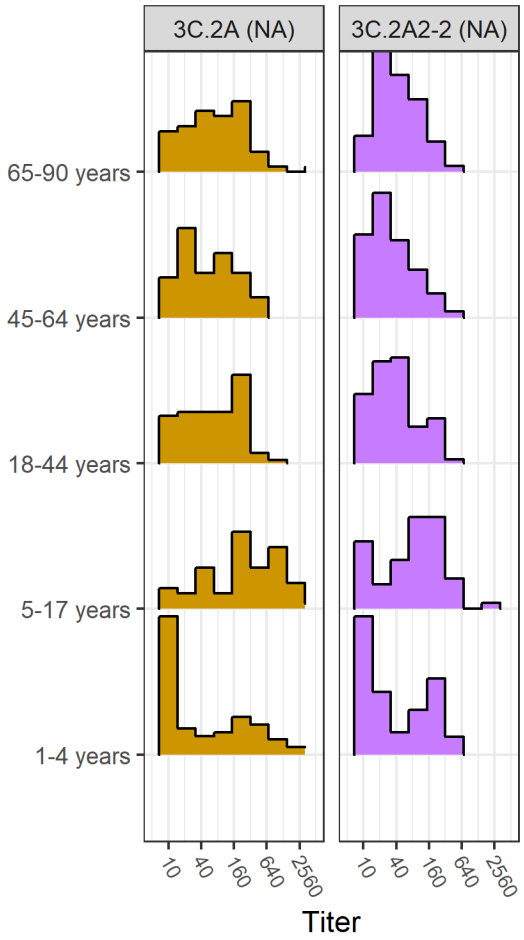

Fig S3. Distribution of NA titers for each strain by age group. A titer of 10 indicates the titer is below the limit of detection.

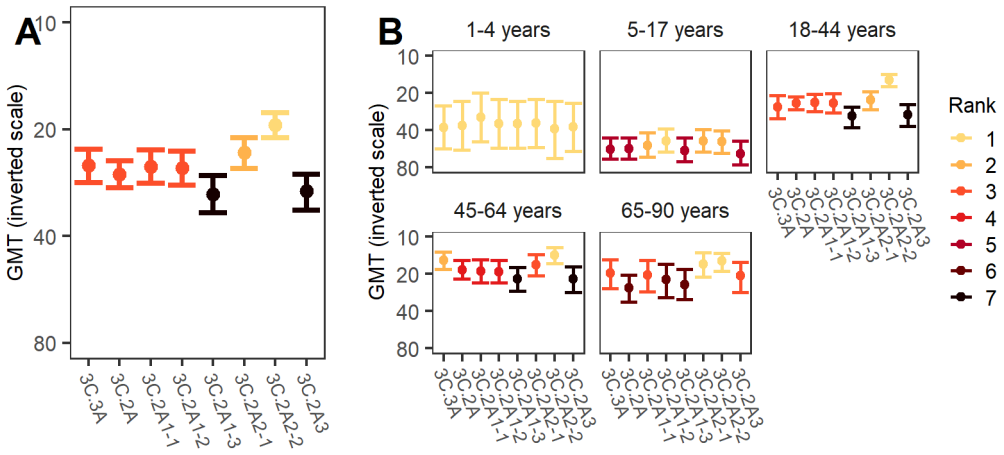

Fig S4. The inferred relative susceptibility for each HA reference strain calculated using geometric mean titers (GMT). Since lower GMT corresponds to higher susceptibility, we use an inverse scale to show the relative susceptibility. Lower ranks (closer to 1) indicate greater susceptibility.

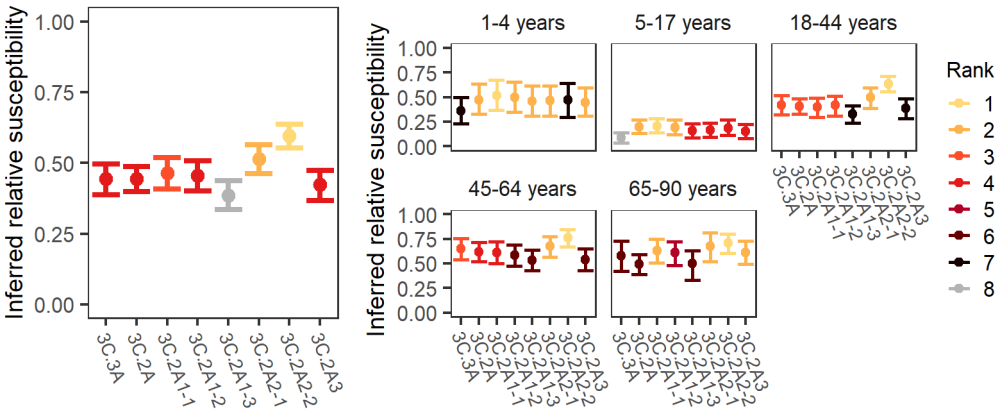

Fig S5. The inferred relative susceptibility and its rank to each HA reference strain using a 1:20 titer threshold. Inferred relative susceptibility and its rank to each reference strain for the whole population (left) and by age group (right). The bars indicate 95% CIs obtained from bootstrapping. Lower ranks (closer to 1) indicate greater susceptibility.

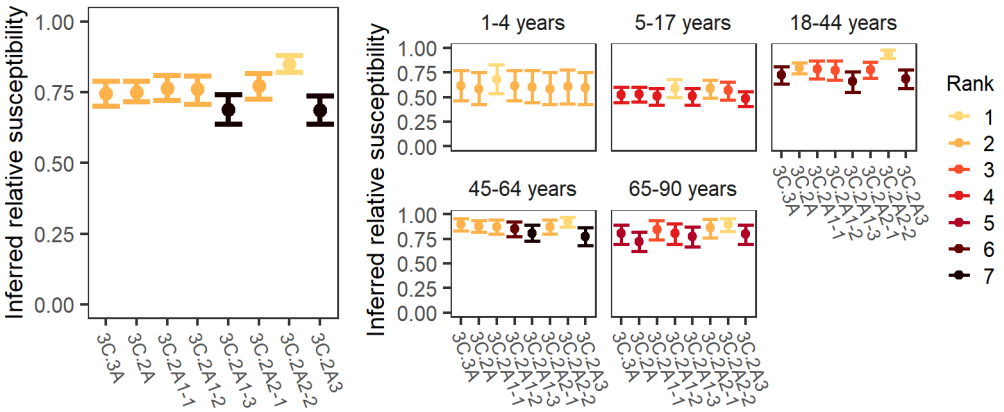

Fig S6. The inferred relative susceptibility and its rank to each HA reference strain using a 1:80 titer threshold. Inferred relative susceptibility and its rank to each reference strain for the whole population (left) and by age group (right). The bars indicate 95% CIs obtained from bootstrapping. Lower ranks (closer to 1) indicate greater susceptibility.

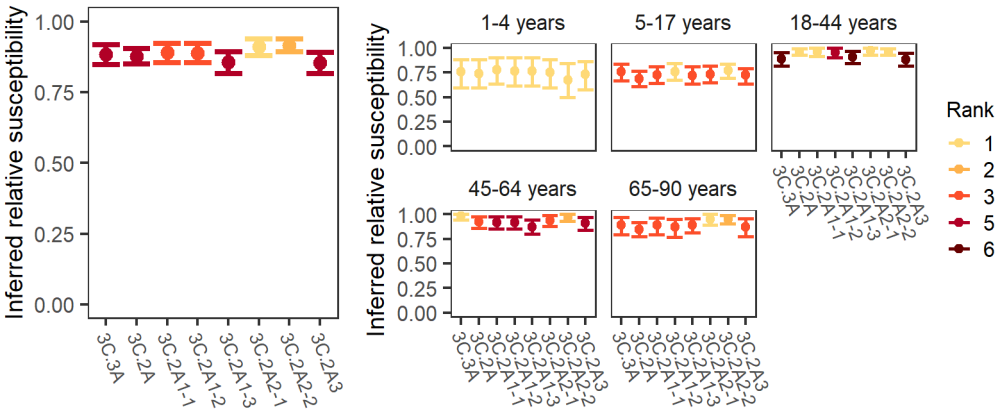

Fig S7. The inferred relative susceptibility and its rank to each HA reference strain using a 1:160 titer threshold. Inferred relative susceptibility and its rank to each reference strain for the whole population (left) and by age group (right). The bars indicate 95% CIs obtained from bootstrapping. Lower ranks (closer to 1) indicate greater susceptibility.

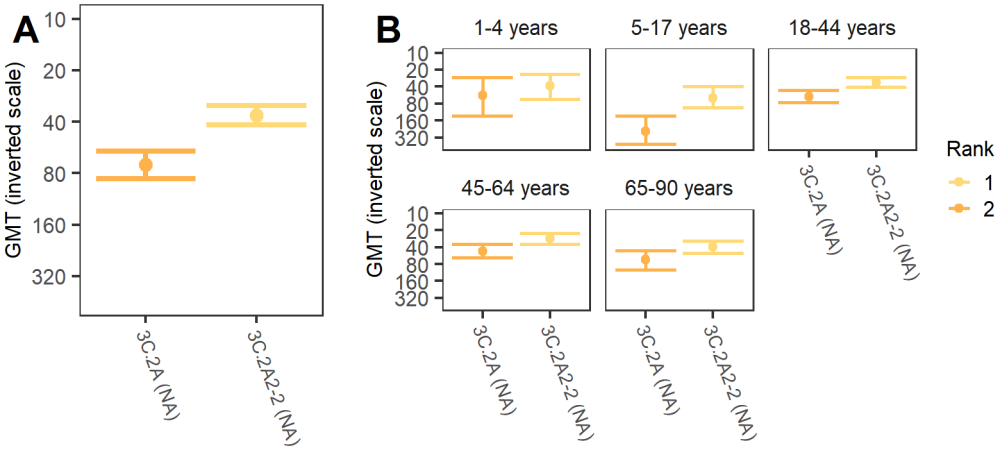

Fig S8. The relative susceptibility for each NA strain calculated using geometric mean titer(GMT). Since lower GMT corresponds to higher susceptibility, we use an inverse scale to show the relative susceptibility. The bars indicate 95% CIs obtained from bootstrapping. The lower rank (rank 1) indicates significantly higher susceptibility.

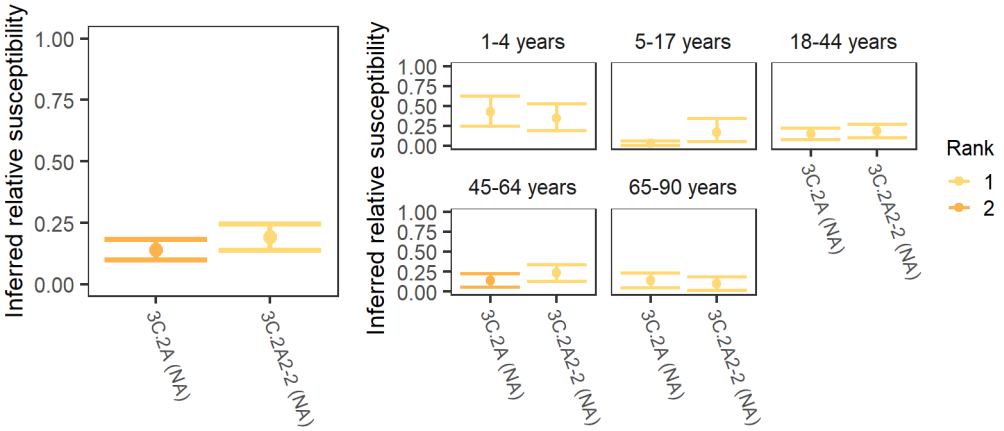

Fig S9. The inferred relative susceptibility and its rank to each NA reference strain using a 1:20 threshold. Inferred relative susceptibility and its rank to each reference strain for the whole population (left) and by age group (right). The bars indicate 95% CIs obtained from bootstrapping. The lower rank (rank 1) indicates significantly higher susceptibility.

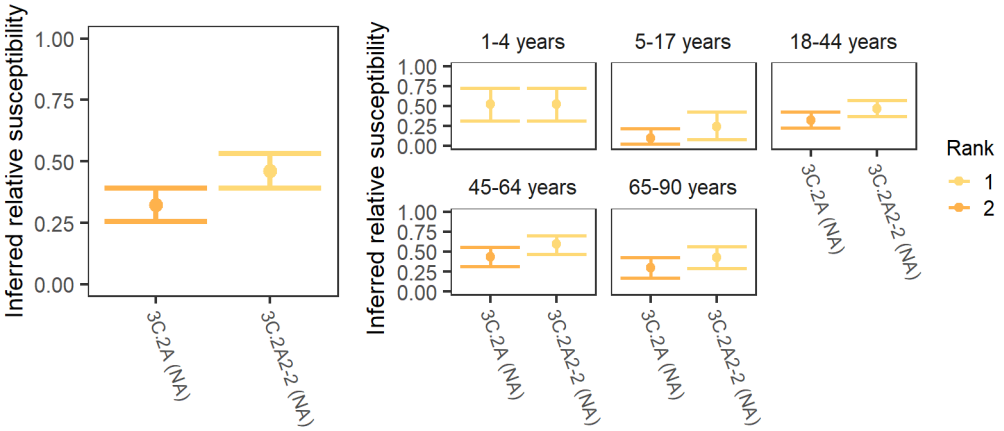

Fig S10. The inferred relative susceptibility and its rank to each NA reference strain using a 1:40 titer threshold. Inferred relative susceptibility and its rank to each reference strain for the whole population (left) and by age group (right). The bars indicate 95% CIs obtained from bootstrapping. The lower rank (rank 1) indicates significantly higher susceptibility.

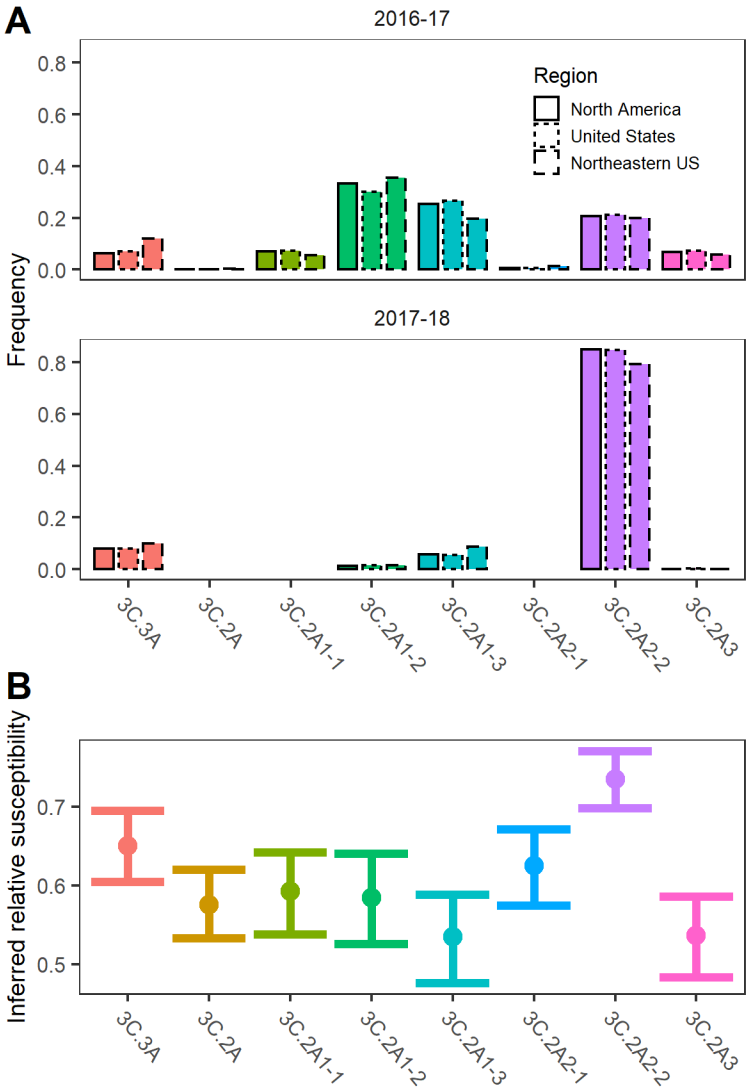

Fig S11. Comparison of H3 frequencies by clade (reference strain) and inferred relative susceptibilities. A. Frequencies of H3 sequences assigned to each test virus were calculated using GISAID sequences from North America, US, and the Northeastern US during the 2016-17 and 2017-18 season. B. Inferred relative susceptibilities to test viruses.

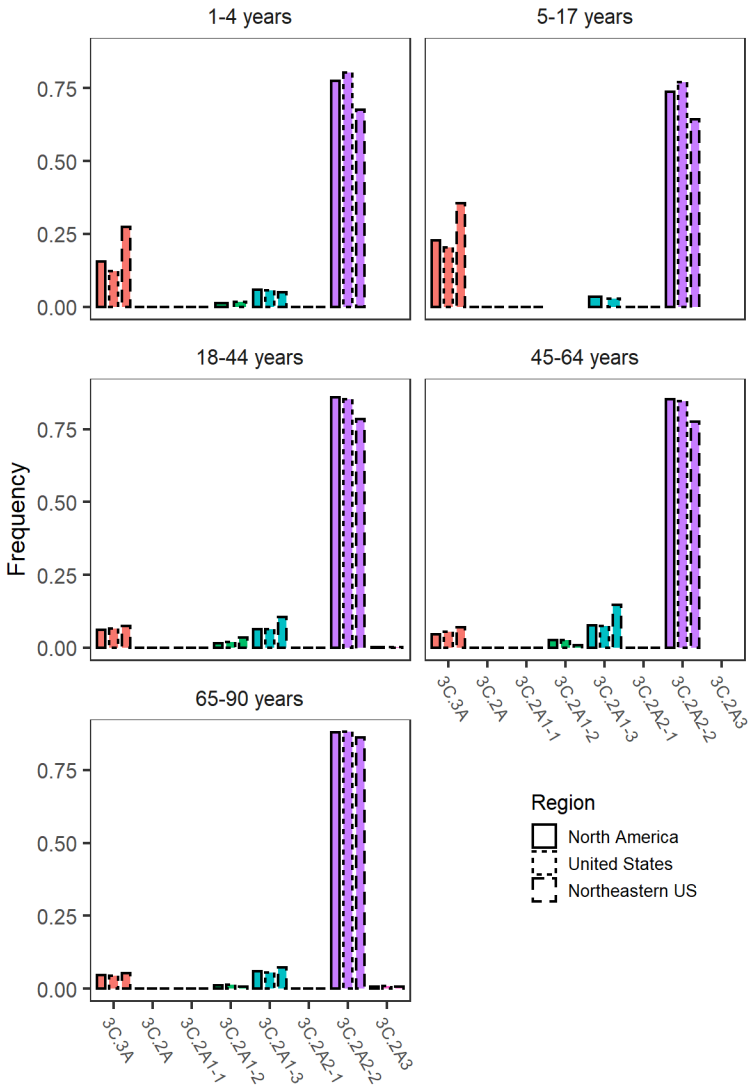

Fig S12. Frequencies of H3 sequences in the 2017-18 season assigned to each reference virus by age group. Frequencies were calculated using GISAID sequences collected in North America, US, and the Northeastern US, respectively.

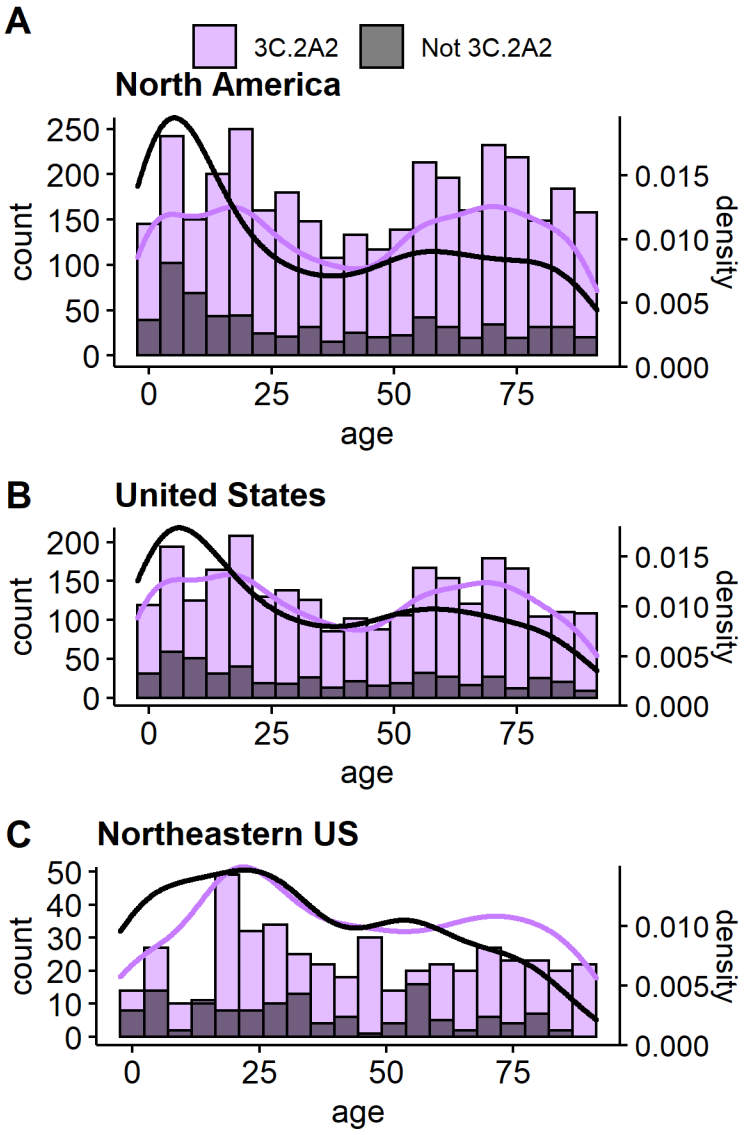

Fig S13. Age distributions of 3C.2A2-2-associated and other reference strains in the 2017-18 season. Strains from GISAID were characterized as belonging to the 3C.2A2 clade or not. Lines show the respective densities.

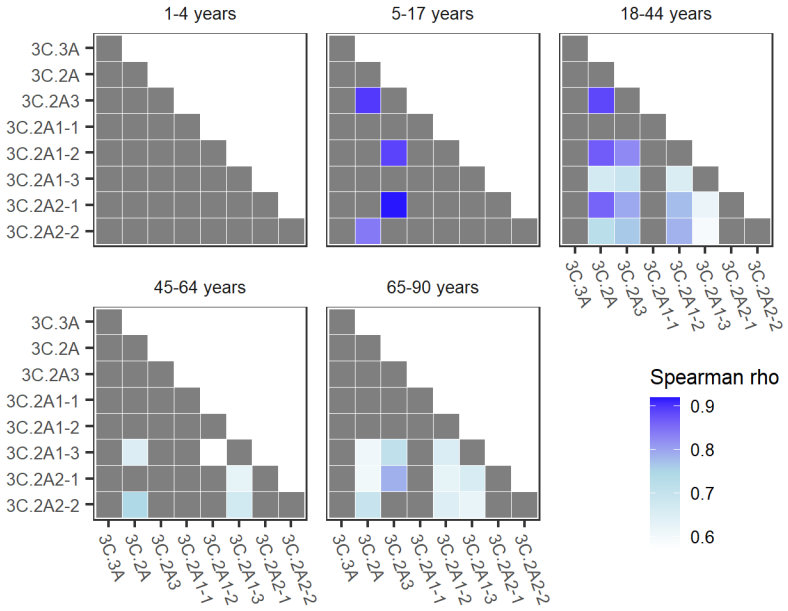

Fig S14. Compared to the youngest age group, older children and adults have significantly more weakly correlated titers to different strains. For each pair of viruses, the correlation between HA titers was calculated. The cells are colored blue if the correlation is significantly weaker in the age group compared to the same pair in 1- to 4-year-olds. Individuals with undetectable titers have been removed.

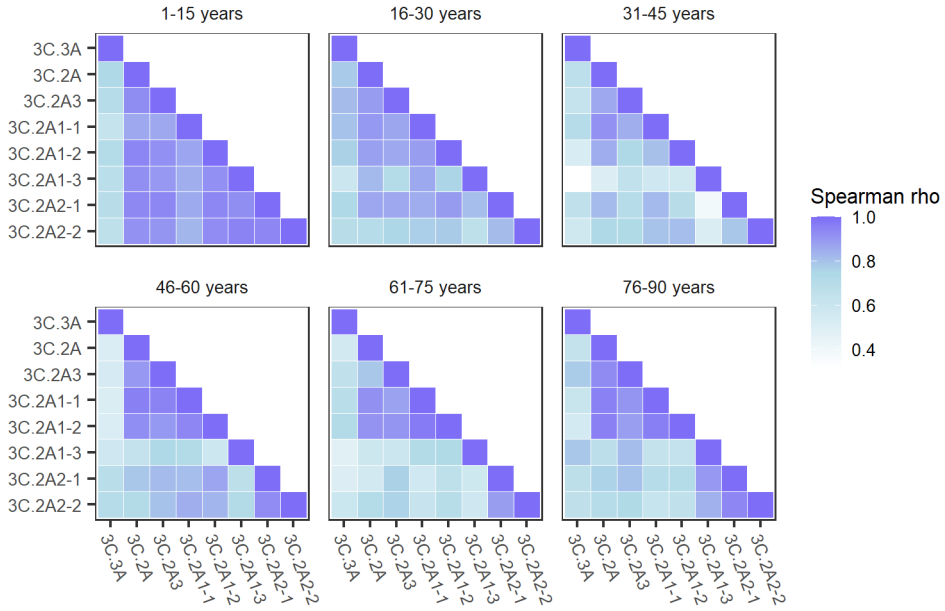

Fig S15. Correlations between titers to different test viruses by age group with equal number of years. For each pair of viruses, the correlation between HA titers was calculated. Individuals with undetectable titers have been removed.

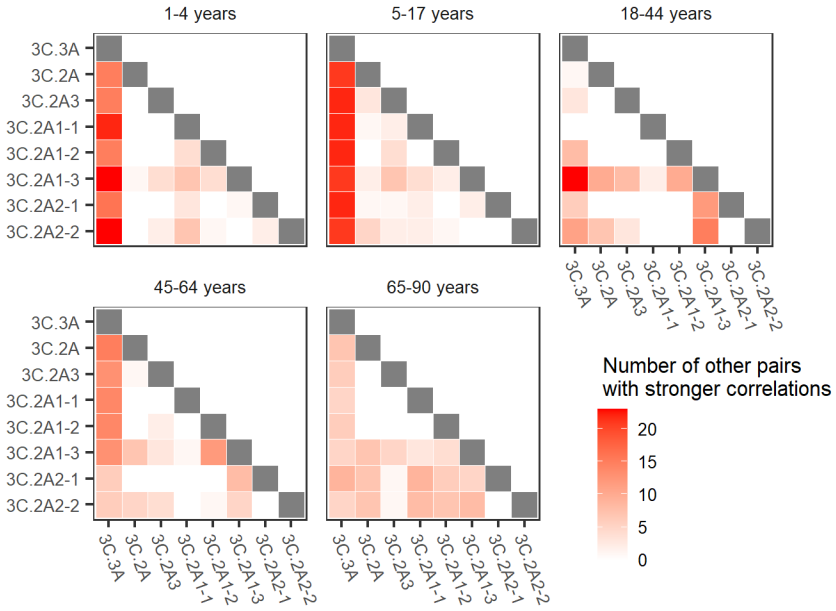

Fig S16. Weakly correlated reference pairs by age group. For each pair of reference viruses, the correlation between HA titers was calculated. The correlation coefficients of the virus pairs within each age group were compared to each other to test whether one correlation was significantly weaker than the other. Then, for each virus pair, the number of comparisons in which the pair's correlation was significantly weaker than that of other pairs (within that age group) was counted. Stronger colors indicate virus pairs with especially weak correlations.

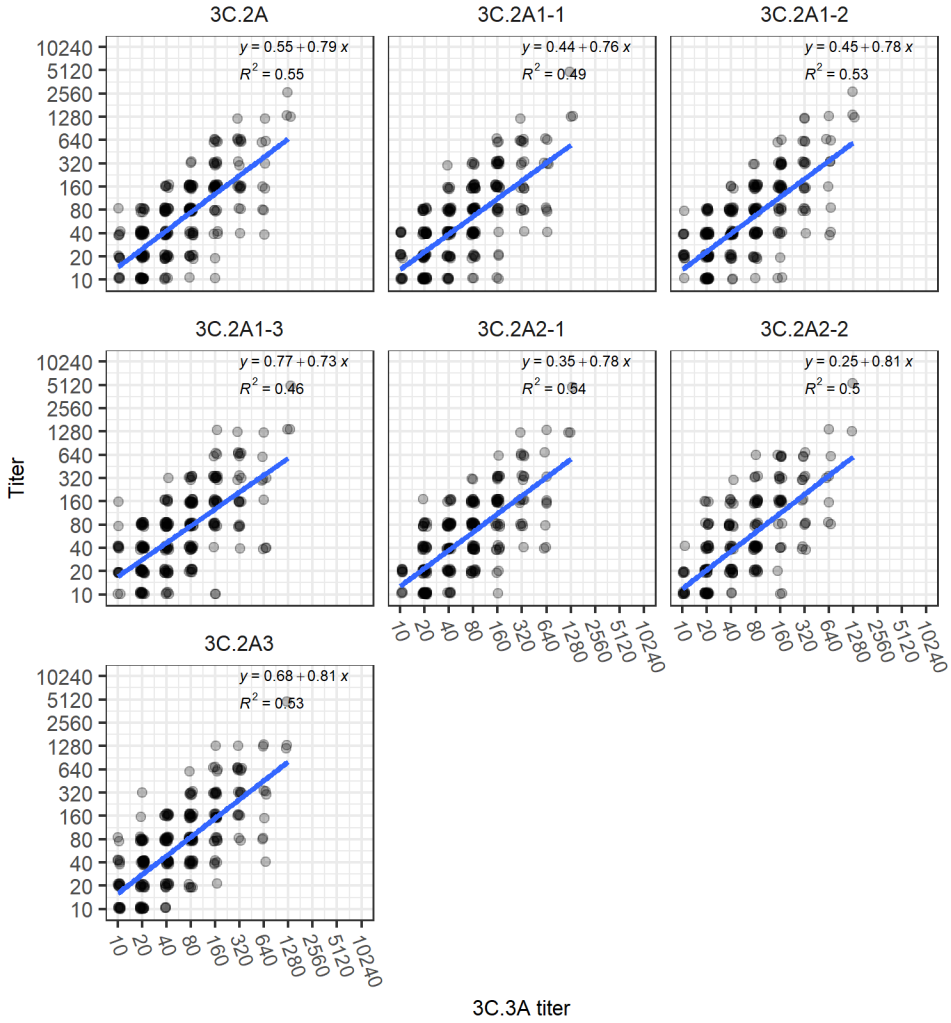

Fig S17. Correlations between 3C.3A titers and other titers in all ages. Points are slightly jittered. Blue line indicates the regression line. Individuals with undetectable titers to all strains were removed from the analysis.

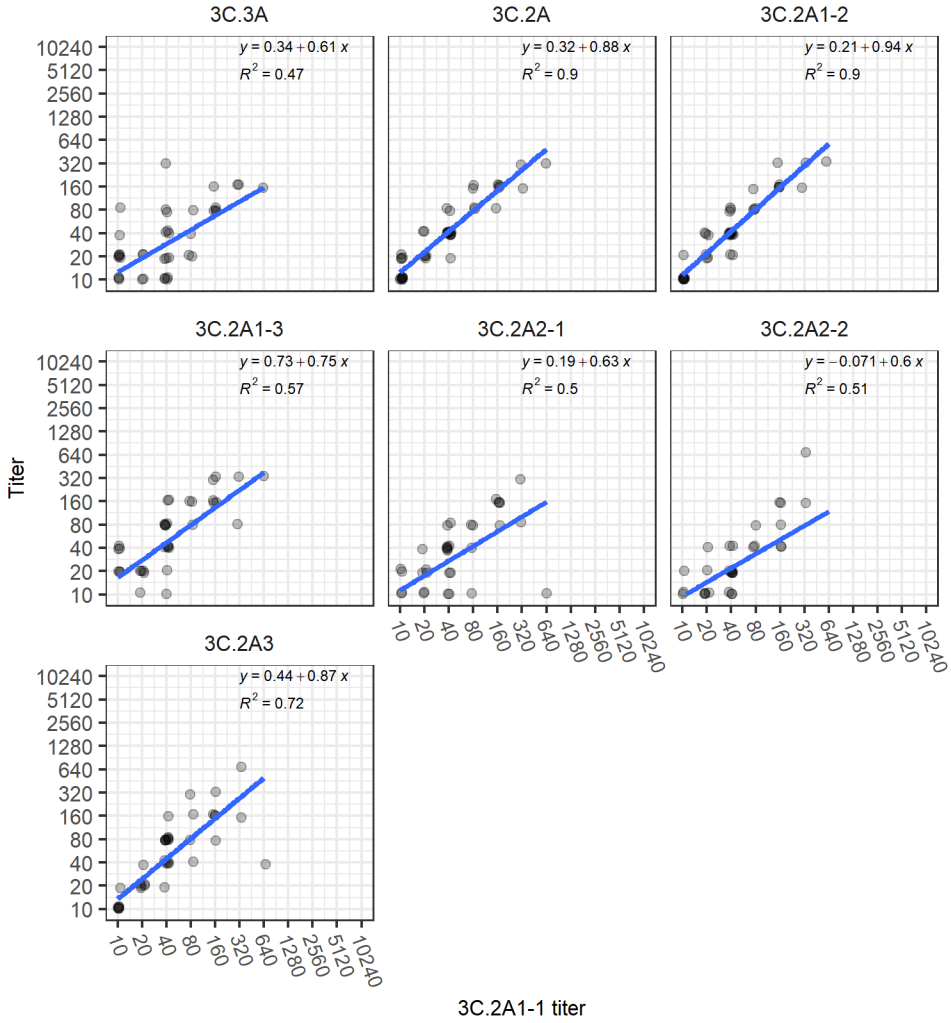

Fig S18. Correlation between 3C.2A1-1 titers and other titers in 45- to 90-year-olds. Points are slightly jittered. Blue line indicates the regression line. Individuals with undetectable titers to all strains were removed from the analysis.

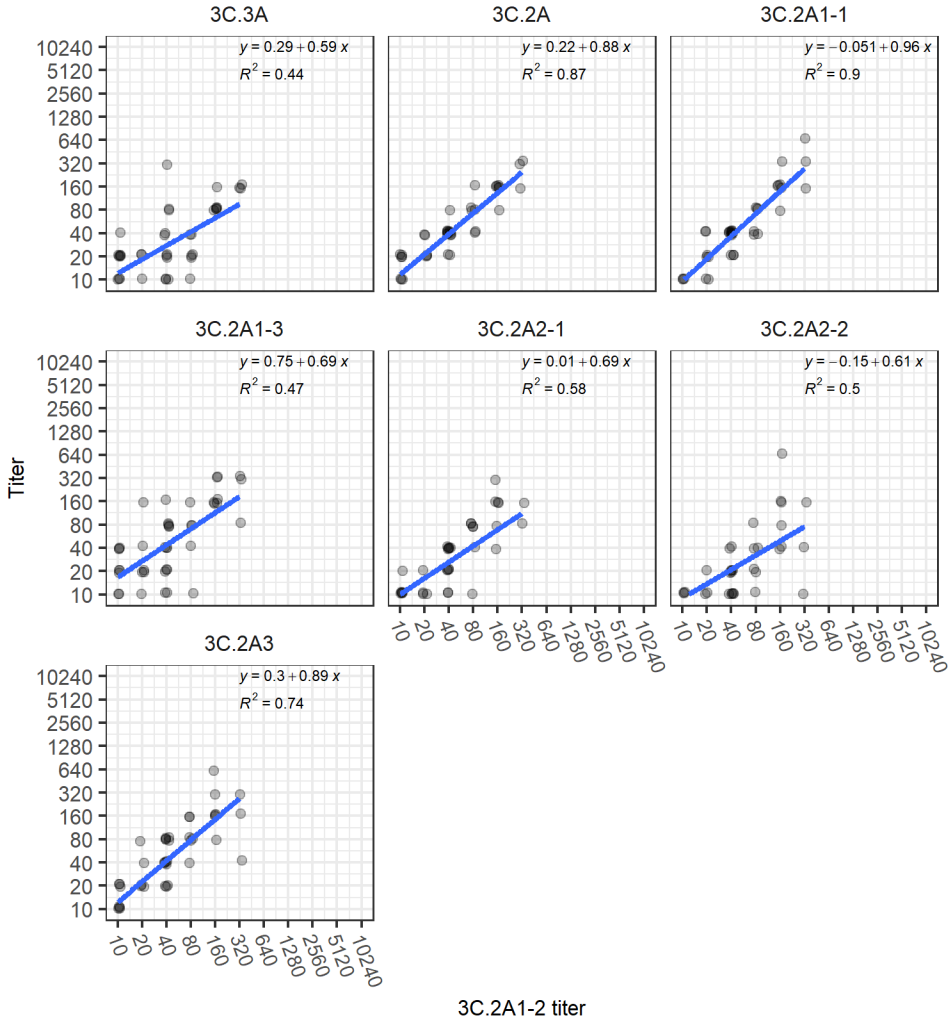

Fig S19. Correlations between 3C.2A1-2 titers and other titers in 45- to 90-year-olds. Points are slightly jittered. Blue line indicates the regression line. Individuals with undetectable titers to all strains were removed from the analysis.

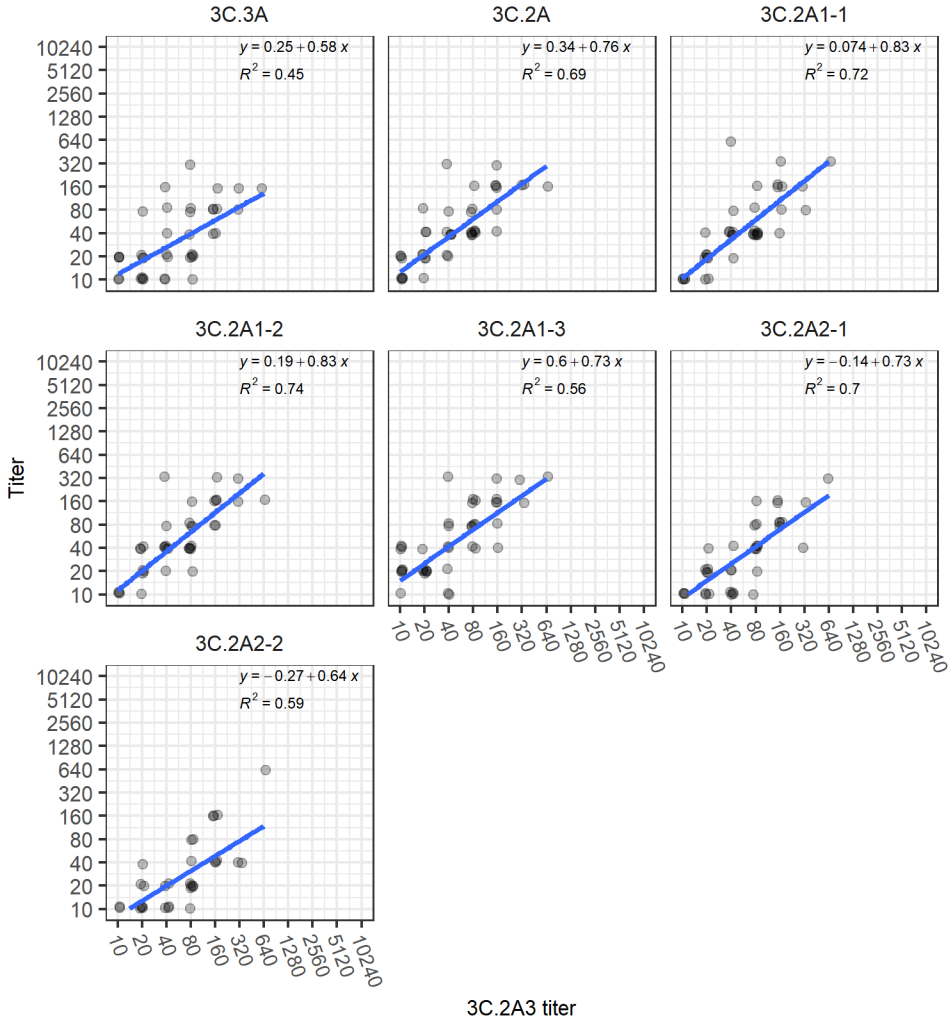

Fig S20. Correlations between 3C.2A3 titers and other titers in 45- to 90-year-olds. Points are slightly jittered. Blue line indicates the regression line. Individuals with undetectable titers to all strains were removed from the analysis.

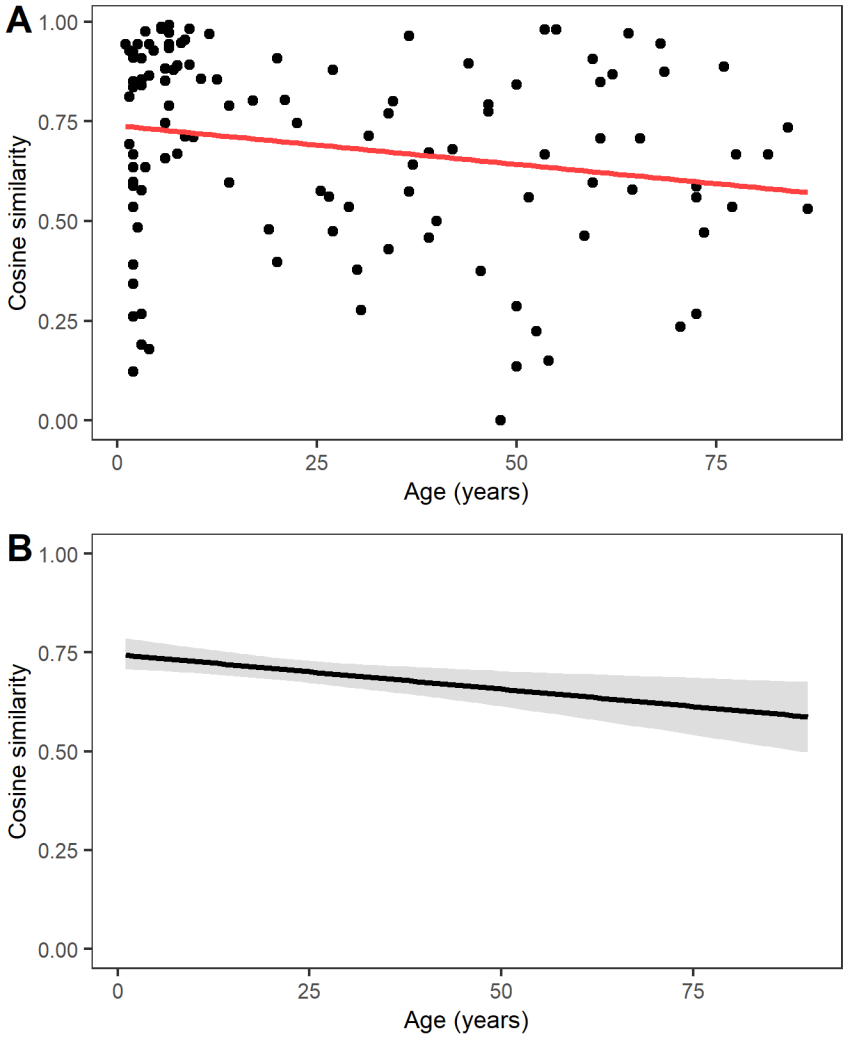

Fig S21. The similarity of HA-NA titer vectors declines with age. A. Cosine similarities of HA-NA titers between pairs of individuals (points) and the regression line (line). Each cosine similarity was calculated from a random pair of individuals within a 3-year age difference. B. The distribution of trends in cosine similarity by age obtained by regressing cosine similarity by age in 1000 different random pairings. The line indicates the mean of the 1000 regression lines, and the shade indicates the 95% interval of the regression lines.

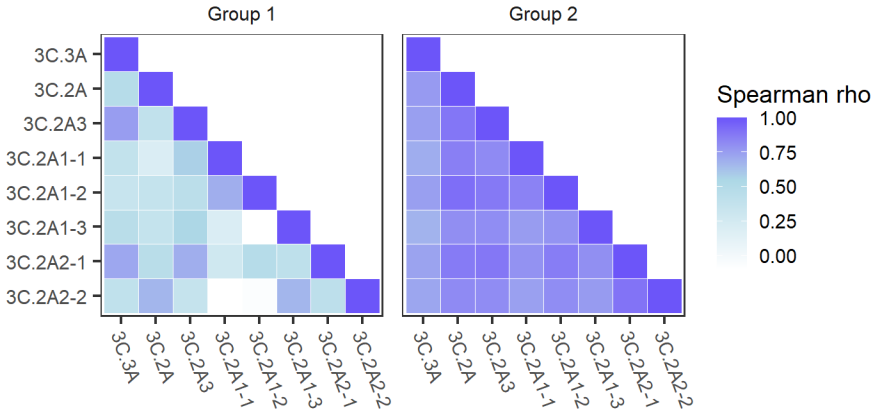

Fig S22. Correlations between titers to different strains within each group. Each cell is colored by the correlation coefficient. Individuals with undetectable titers to all reference viruses have been removed.

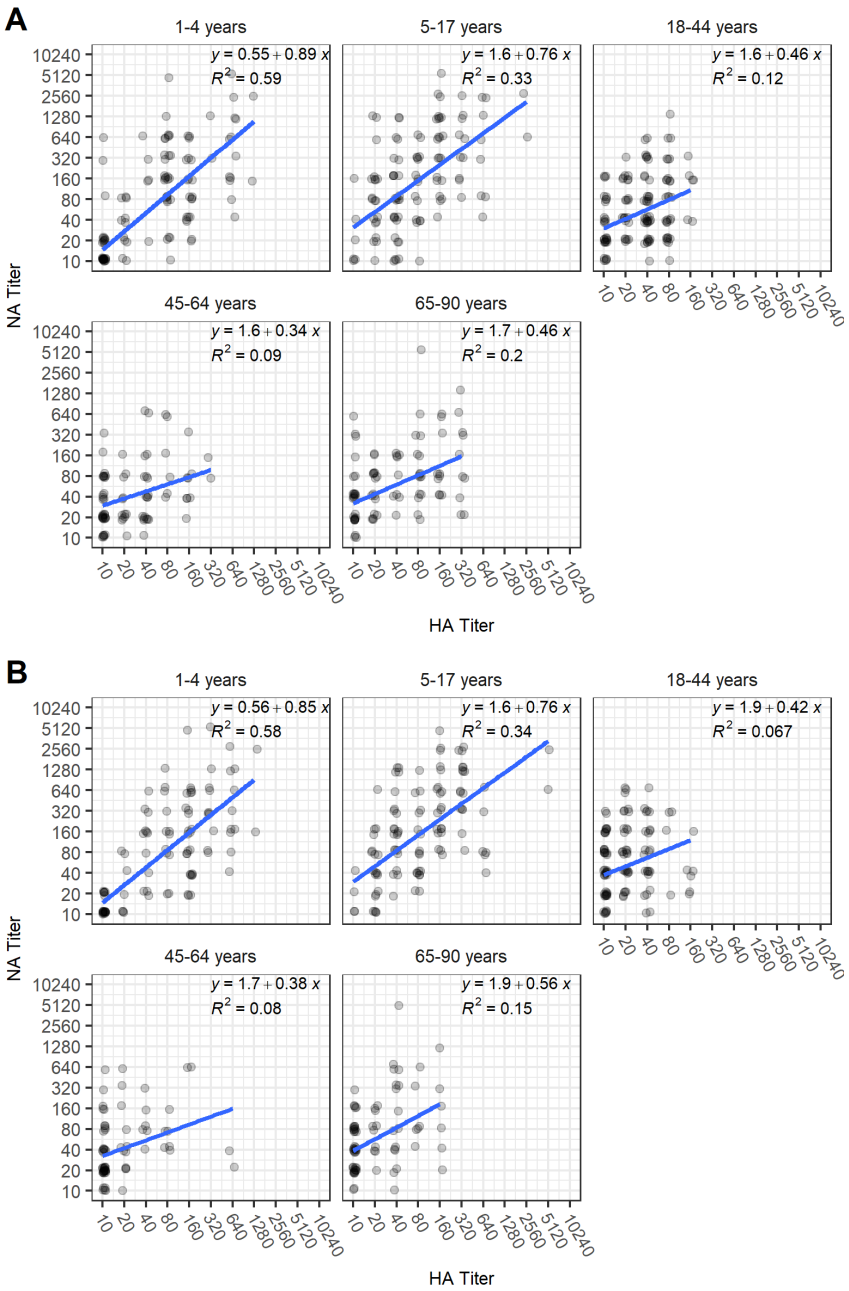

Fig S23. Correlations between HA and NA titers A. Titers to 3C.2A HA and NA. B. Titers to 3C.2A2 HA and NA. Points have been slightly jittered to show density. Blue lines indicate the regression lines.

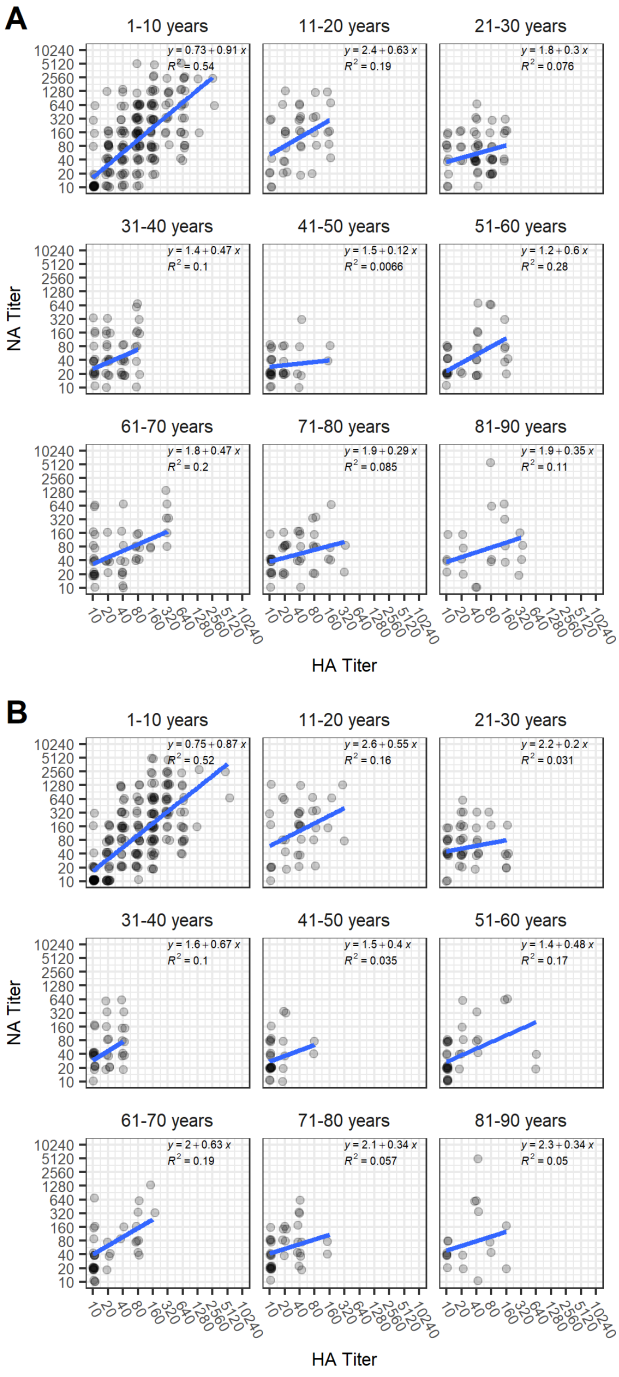

Fig S24. Correlations between HA and NA titers by 10-year age bins
A.Titers to 3C.2A HA and NA. B. Titers to 3C.2A2 HA and NA. Points have been slightly jittered to show density. Blue lines indicate the regression lines.